Chromatin activity of IκBα mediates the exit from naïve pluripotency

Luis G. Palma[1,2,3,δ], Daniel Álvarez-Villanueva[1,4,δ], María Maqueda[1,2,3], Mercedes Barrero[5], Arnau Iglesias[1,2,3], Joan Bertran[6], Damiana Álvarez-Errico[2], Carlos A. García-Prieto[2], Cecilia Ballaré[5], Virginia Rodriguez-Cortez[2], Clara Bueno[2], August Vidal[4], Alberto Villanueva[7], Pablo Menéndez[2,3,8,9,10], Gregoire Stik[2], Luciano Di Croce[5,10,11], Bernhard Payer[5,11], Manel Esteller[2,3,10,12], Lluís Espinosa[1,3,*] & Anna Bigas[1,2,3,*]

[1]Program in Cancer Research. Hospital del Mar Research Institute, Barcelona, Spain.

[2]Josep Carreras Leukemia Research Institute, Barcelona Spain.

[3]Centro de Investigación Biomédica en Red Cancer (CIBERONC), Madrid, Spain.

[4]Institut Investigació Biomèdica de Bellvitge (IDIBELL), L'Hospitalet de Llobregat, Barcelona, Spain.

[5]Centre for Genomic Regulation (CRG), The Barcelona Institute of Science and Technology, Barcelona, Spain.

[6]Faculty of Sciences, Technology and Engineering, Universitat de Vic - Universitat Central de Catalunya, Vic 08500 Spain

[7]Catalan Institute of Oncology (ICO/IDIBELL), L'Hospitalet de Llobregat, Barcelona, Spain.

[8]Spanish Network for Advanced Therapies (RICORS-TERAV). Carlos III Health Institute (ISCIII), Spain.

[9]Department of Biomedicine. University of Barcelona, Spain.

[10]Institucio Catalana de Recerca i Estudis Avançats (ICREA), Barcelona, Spain.

[11] Universitat Pompeu Fabra, Barcelona, Spain.

[12]Physiological Sciences Department, School of Medicine and Health Sciences, University of Barcelona (UB), Barcelona, Catalonia, Spain.

[δ]These authors contributed equally

Keywords: IκBα, NFKBIA, NF-κB, DNA Methylation, Polycomb, Embryonic Stem Cells, Pluripotency Exit, Germ Layer Specification,

**Corresponding authors:*

28 Anna Bigas and Lluis Espinosa

29 Cancer Research Program. CIBERONC.

30 Hospital del Mar Research Institute

31 Doctor Aiguader 88, 08003, Spain.

32 Tel: +34 933160440; email: abigas@researchmar.net; lespinosa@researchmar.net

33 **Summary**

34 Maintenance of pluripotency is a multifactorial process in which NF-κB is a negative regulator. Our
35 previous work identified a chromatin role for IκBα, the master regulator of NF-κB signaling, that is
36 critical for the proper regulation of various tissue stem cells. Here, we found that IκBα accumulates
37 specifically in the chromatin fraction of pluripotent embryonic stem cells. IκBα depletion does not
38 affect NF-kB-dependent transcription, but causes a profound epigenetic rewiring in pluripotent stem
39 cells, including alterations in H3K27me3, a histone mark catalyzed by Polycomb repression complex
40 2. Chromatin changes induced by IκBα depletion affect a subset of pluripotency genes and are
41 associated with altered gene transcription. At the cellular level, IκBα-deficient embryonic stem cells
42 are arrested in a naive pluripotency state when cultured in serum/LIF conditions and fail to exit
43 pluripotency under differentiation conditions. By constructing separation-of-function mutants, we
44 show that the effects of IκBα in regulating stem cell pluripotency are NF-κB-independent, but mainly
45 rely on its chromatin-related function. Taken together, our results reveal a novel mechanism by which
46 IκBα participates in the regulation of the pluripotent state of embryonic stem cells and shed light on
47 the interplay between inflammatory signals and the regulation of pluripotency.

INTRODUCTION

Embryonic Stem Cells (ESCs) pluripotency is characterized by the capacity to generate all somatic and germline lineages both *in vitro* and *in vivo*, depending on the culture conditions. When cultured in serum plus Leukemia Inhibitory Factor (LIF) (Serum/LIF), murine ESCs (mESCs) include cells interconverting to different metastable states [1] that either resemble preimplantation blastocyst (naïve pluripotency) or post-implantation (primed pluripotency) embryonic stages [2–5]. The heterogeneity of mESCs in Serum/LIF is reduced by culturing them in the presence of GSK3β and MEK1/2 inhibitors (CHIR99021 and PD0325901, respectively) along with LIF (2i/LIF). Under these conditions, mESCs enter a ground state of naïve pluripotency characterized by self-renewal activity while suppressing any pro-differentiating signals [6,7]. This pluripotent state closely resembles the inner cell mass of the E4.0 mouse preimplantation blastocyst [8]. After implantation, pluripotent capability of the mouse embryo (E5.5) becomes restricted to Epiblast Stem Cells (EpiSCs), which represent a primed pluripotent state, characterized by coexpression of pluripotency and lineage specification markers [9,10]. EpiSCs can give rise to cells from the three germ layers (endoderm, mesoderm and ectoderm), albeit their contribution to chimeras or to germ cells is greatly compromised [4,11]. EpiSCs can be derived *in vitro* from naïve pluripotent cells when cultured in a medium supplemented with Nodal and fibroblast growth factor (FGF) [12]. Different epigenetic features distinguish naïve from primed pluripotent states [13], such as changes in the X chromosome inactivation in female cells [12,14], histone post-translational modifications [10] or a global DNA hypomethylation profile observed in naïve pluripotent stem cells [15–17]. These epigenetic changes are a prerequisite for the subsequent activation of gene circuits associated with pluripotency exit and germ layer specification [9,10]. Crucial regulatory elements for the transition from naïve to primed pluripotency state are located in distal DNA regions or enhancers to facilitate the resolution toward the primed state [18,19]. Therefore, identifying novel players to fine-tune the equilibrium between ground and primed states is crucial for preserving both pluripotency stability and differentiation capability in mESCs.

There is now strong evidence that inflammatory signals are critical for stem cell development [20–22], with NF-κB being the main effector. Different strategies to inhibit or attenuate NF-κB in ESCs lead to increase pluripotency gene expression and impair cell differentiation [23,24], or it facilitates reprogramming to induced pluripotent stem cells (iPSC) [25]. Canonical NF-κB signaling is triggered by the IKK kinase complex, which induce the phosphorylation and subsequent degradation of the NF-κB inhibitor, IκBα, leading to nuclear translocation of the NF-κB factors (e.g. p50/p65) [26]. However, we have previously identified a nuclear IκBα function, which is critical for tissue stem cell homeostasis and the proper differentiation of epidermal, intestinal and hematopoietic stem cells [27–30]. IκBα chromatin function is mediated by the interaction with histone deacetylases (HDACs), core elements of the Polycomb Repressor Complex 2 (PRC2) and histone H2A and H4 [27,29,31].

We have now investigated the role of IκBα in the context of pluripotent stem cells. Whereas cytoplasmic IκBα is detected in the different states and its levels decrease after differentiation, in agreement with NF-κB activity as a promoter of differentiation, we specifically detected chromatin-bound IκBα in the naïve pluripotent stem cells. Importantly, IκBα depletion in ESCs did not affect NF-κB activity but it stabilizes the naïve (2i/LIF-like) state of pluripotency under Serum/LIF conditions, displaying an epigenetic rewiring, including changes in the PRC2-dependent H3K27me3 histone mark and impacting in proximal and distal regulation of pluripotent genes. Using a new Separation-Of-Function (SOF) IκBα mutants[32], we have now definitively demonstrated that chromatin-bound IκBα is required for naïve pluripotency exit of mESCs in an NF-κB-independent manner. Overall, we identified IκBα as a novel key player in the regulation of the exit from naïve-to-primed pluripotency and essential for the activation of gene programs involved in germ layer specification.

98 **RESULTS**

99 **IκBα and NF-κB have opposite expression dynamics in naïve pluripotent cells**

100 Due to the prominent role of NF-κB signaling in mESCs regulation, we analyzed the expression
101 pattern of the different NF-κB members including the IκB inhibitors in the three defined
102 pluripotent stages: ground state of naïve pluripotency (2i/LIF), naïve pluripotency
103 (Serum/LIF), and primed pluripotency (Epiblast Stem Cells or EpiSCs) [5] (Figure 1A). In
104 agreement with NF-κB being a pro-differentiation factor, canonical NF-κB inhibitors including
105 IκBα (*Nfkbia*), IκBβ (*Nfkbib*) and IκBε (*Nfkbie*) were all expressed in the naïve pluripotency
106 state (both 2i/LIF and Serum/LIF), with *Nfkbia* levels gradually reduced upon naïve
107 pluripotency exit towards EpiSCs (Figure 1B). In contrast, *Rela, Nfkb1 and Nfkb2* genes,
108 codifying for the NF-κB factors p65/RelA, p105 and p100, respectively, showed opposite
109 expression dynamics increasing the levels in EpiSCs (Figure 1C). We further characterized the
110 distribution of IκBα in the cytoplasm, nucleus and chromatin fractions of the three states of
111 pluripotency (Figure 1D). Total IκBα protein levels correlated with the detected RNA levels in
112 the three different cellular states being highest in the 2i/LIF condition (Figure 1B), with a large
113 accumulation in the cytoplasm. A fraction of IκBα protein was detected in the chromatin of
114 naïve pluripotent cells, being highest in cells cultured in Serum/LIF conditions compared to
115 2i/LIF and absent in the EpiSCs. (Figure 1D). The dynamics of IκBα RNA and protein levels from
116 naïve pluripotent ESCs to EpiSCs was further corroborated by analysis of an additional
117 database that includes both naïve and primed pluripotent states[33] (Figure 1E).

118 Next, we studied IκBα expression in differentiated embryoid bodies (EBs) from mESCs
119 (Serum/LIF) (see materials and methods) and analyzed the expression levels of different
120 pluripotency, differentiation-linked, and NF-κB genes by RNA sequencing. *Nfkbia* (IκBα gene)
121 was expressed at higher levels specifically in mESCs (Serum/LIF) whereas cells undergoing
122 differentiation (48h and 96h) displayed a reduction in its expression levels (Figure 1F). The
123 expression pattern of *Nfkbia* was similar to the pluripotency genes whereas most of the NF-
124 κB genes were upregulated upon differentiation, clustering together with developmental
125 genes, as previously described [24]. Notably, several polycomb elements were highly expressed
126 in mESCs, consistent with the possibility that chromatin-bound IκBα modulates PRC2 activity
127 [27] in the pluripotent state.

128 Taken together, these data show that, unlike the other NF-kB inhibitors and target genes, the
129 expression of *Nfkbia* is high in the naive pluripotent state, with IκBα protein present in the
130 cytoplasm and chromatin of naive pluripotent cells. Moreover, whereas canonical NF-κB
131 subunits are primarily absent, we detected several Polycomb elements expressed in mESCs.

132 **IκBα is required in mESCs to exit the naïve pluripotency state**

133 To investigate the functional implication of IκBα in naïve pluripotency, we knocked-out (KO)
134 IκBα protein in mESCs by CRISPR-Cas9 (IκBα-KO mESCs) (Figure S1A and materials and

135 methods). Notably, IκBα KO mESCs have an impaired ability to undergo differentiation and
136 cannot properly switch off the pluripotency program after 216h (9 days) of pro-differentiation
137 signals, as it is demonstrated by high levels of pluripotency markers OCT3/4 and NANOG (Fig
138 1A and Fig S1C), higher number of alkaline phosphatase cells (Fig 1B and Fig S1) and higher
139 percentage of SSEA-1^{+} cells (Fig S1B) within the 216h EBs. These results were also supported
140 by the detection of increased expression level of the naïve pluripotency genes *Pou5f1 (Oct3/4*
141 *gene), Gbx2, Klf2, Sox2, Zfp42 (Rex1)* and *Nanog* in IκBα KO EBs after 216h of differentiation
142 (Figure S1B).

143 To shed light into the molecular mechanisms governing the differentiation impairment in IκBα
144 KO EBs, we performed RNA-seq of IκBα WT and IκBα KO mESCs in the first stages of the
145 embryoid body differentiation. Analysis of the data indicated that IκBα KO EBs cannot
146 successfully evolve towards differentiation trajectories, as shown by principal component
147 analysis (PCA) of IκBα-WT and IκBα-KO EBs at 48h and 96h in differentiation media (Figure
148 2C). Analysis of naïve pluripotency markers at 96h (*Gab1, Sox2, Esrrb, Zfp42, Dppa4, Klf2,*
149 *Prdm14, Klf4, Tfcp2l1*) also showed higher expression levels in IκBα KO compared to their IκBα
150 WT counterparts (Figures 2D and S1F). Defective differentiation capacity of IκBα KO EBs
151 involved programs associated with specification of all 3 germ layers (endoderm, mesoderm,
152 and ectoderm) (Figures 2E-G). Moreover, IκBα KO EBs were smaller in size (Figure S1E), in
153 agreement with the reduced developmental potential of IκBα-depleted mESCs [34]. To further
154 study the requirement of IκBα in pluripotency exit *in vivo*, we established teratomas by
155 subcutaneous injection of IκBα-WT and IκBα-KO mESCs (Figure 2H and materials and
156 methods) into NSG (NOD.Cg-Prkdc^{scid} Il2rg^{tm1Wjl}/SzJ) mice. IκBα-KO teratomas showed a
157 decreased differentiation potential, as indicated by higher number of OCT4^{+} cells 6 weeks
158 after injection (Figures 2H-J). These observations further confirm the essential role of IκBα in
159 the exit from the pluripotency state not only *in vitro* but also under *in vivo* differentiation
160 signals. To understand the conditions in which IκBα is required for pluripotency exit, we
161 differentiated IκBα-WT and IκBα-KO mESCs cultured in Serum/LIF (naïve pluripotency)
162 towards EpiSCs (primed pluripotency) (Figure 3A, upper panel). IκBα-KO cells were not
163 committed towards the primed pluripotency stage and maintained an elevated expression
164 levels of naïve pluripotency genes (*Dppa3, Nanog, Sox2, Rex1, Klf2, Klf4, Gbx2, Tbx3*) (Figure
165 3A, bottom panel). Additionally, IκBα-KO cells retained a naïve pluripotent morphology,
166 forming tight clusters that resemble cells cultured in 2i/LIF medium (Figure S2A).

167 mESCs cultured in serum/LIF are highly heterogeneous, comprising a mixture of cell states
168 that resemble developmental transitions from preimplantation (naïve pluripotency) to
169 postimplantation (primed pluripotency) embryo [2,3]. To investigate how IκBα deficiency was
170 affecting the exit of mESCs from naïve pluripotency, we performed a Gene Set Enrichment
171 Analysis (GSEA) using RNA-seq data from IκBα-KO and IκBα-WT mESCs cultured in Serum/LIF
172 against gene signatures for 2i/LIF and Serum/LIF pluripotency [35]. GSEA results revealed a
173 significant enrichment in Serum/LIF IκBα-KO mESCs transcriptome for genes specifically
174 expressed in the naïve ground state (2i/LIF), while they negatively correlate with mESCs

175 cultured in Serum/LIF (Figure 3B) [35]. These results agree with the fact that IκBα-KO mESCs
176 cultured in Serum/LIF resemble 2i/LIF morphology, with homogeneous tight clusters of cells,
177 whereas IκBα-WT mESCs retain the colony heterogeneity (Figure S2B). Interestingly, the
178 higher levels of ground-state-related genes *Zfp42* (*Rex1*), *Klf2* and *Tbx3* in IκBα-KO mESCs
179 were partially obtained when IκBα-WT mESCs were cultured in 2i/LIF for two consecutive
180 passages (Figure 3C).

181 One of the key features of the naïve pluripotency state is its global DNA hypomethylation
182 pattern [15,16]. We assessed the DNA methylation status of IκBα-WT and IκBα-KO mESCs
183 cultured in Serum/LIF conditions by analysis of 5-methyl-cytosine (5mC) mark and using DNA
184 methylation arrays [36]. We found that IκBα-KO mESCs contained much lower levels of 5mC
185 compared to IκBα-WT cells (Figure 3D). Moreover, DNA methylation arrays confirmed a global
186 pattern of DNA hypomethylation in IκBα-KO mESCs, which was maintained in 96h EBs (Figure
187 3E). Interestingly, the DNA hypomethylation status occurred in a genome-wide fashion
188 affecting all chromosomes (Figure S2C), in accordance with a higher pluripotent state of IκBα-
189 KO mESCs.

190 Overall, these data demonstrate that IκBα is required for the exit of the naïve state of
191 pluripotency and its deficiency results in impaired differentiation of mESCs *in vivo* and *in vitro*.
192 Accordingly, IκBα-KO mESCs cultured in Serum/LIF showed genome-wide pattern of DNA
193 hypomethylation.

194 **Lack of IκBα causes an epigenetic rewiring in pluripotent stem cells to resemble 2i/LIF naïve**
195 **pluripotency in Serum/LIF culture**

196 ChIP Enrichment Analysis (ChEA) of genes identified in our RNA-seq data of IκBα-KO and WT
197 mESCs revealed that differentially expressed genes were putative targets of chromatin
198 regulators including the PRC2 subunit SUZ12 and MTF2 (Figure 4A). We previously described
199 that IκBα is important for the proper deposition of the H3K27me3 mark in different types of
200 tissue stem cells by associating with elements of the PRC2 complex [27,28]. Since 2i/LIF and
201 Serum/LIF states are characterized by important differences in epigenetic marks, we carried
202 out an epigenetic profiling of IκBα-WT and IκBα-KO mESCs cultured in Serum/LIF. We
203 performed chromatin immunoprecipitation followed by sequencing (ChIP-seq) of histone
204 modifications associated with gene activation (H3K4me3) and gene repression (H3K27me3)
205 (Figures 4B and S3A-B). Overall, Serum/LIF IκBα-KO mESCs exhibited a general increased
206 H3K4me3 status and redistribution of the PRC2-catalyzed H3K27me3 mark (Figure 4B).
207 Notably, gain of the H3K4me3 mark was associated with a reduction of H3K27me3 levels in
208 genes associated with naïve pluripotency function (Figures 4B-C and S3A-B). In particular, 41
209 genes with concomitant gain of H3K4me3 and loss of H3K27me3 were found to be enriched
210 in mechanisms associated with pluripotency function (Figure 4C), including Tbx3 and Gbx2
211 (Figure 4D-4E). A second set of pluripotency-related genes showed an increase in H3K4me3

212 without changes in H3K27me3 (Zfp42 or Klf2). Both sets of pluripotency genes showed
213 increased expression in the absence of IκBα (Figure 4H).

214 We next aimed to study whether the lack of IκBα was also affecting distal regulatory regions
215 by analyzing enhancer-associated histone marks in IκBα-WT and IκBα-KO mESCs. We
216 quantified the total amount of H3K27Ac (active enhancer) and H3K4me1 (poised enhancer)
217 by ChIP-seq experiments conducted in both IκBα-WT and IκBα-KO mESCs. Overall, IκBα-KO
218 mESCs showed a reduction in poised enhancers at genes (or related genomic regions)
219 associated with differentiation processes (Figures 4F and S3C) and an increase in active
220 enhancers at genes associated with pluripotency (Figure 4F and S3D), such as Tbx3, Tfcp2l1
221 and Zfp42 (Rex1) (Figure 4G), which positively favors their higher expression in IκBα-KO mESCs
222 (Figure 4H). These results further support that mESCs lacking IκBα are epigenetically
223 remodeled to favor the ground state of naive pluripotency, which may negatively impact on
224 their differentiation potential, similar to that described for other models with stabilized naïve
225 pluripotent state[37,38].

226 **The chromatin function of IκBα in pluripotency exit is independent of classical NF-κB**
227 **activity.**

228 Although previous results from C. elegans [39] and Drosophila [27] support the functional
229 relevance of chromatin-related IκBα function, the investigation of this alternative IκBα
230 activity remains challenging due to the predominant role of this protein in NF-κB regulation.
231 However, and similar to that found in other models, we did not detect major changes in
232 canonical NF-κB target genes upon IκBα depletion neither in Serum/LIF mESCs, nor 48h and
233 96h EB-differentiating conditions (Figure 5A). Thus, either NF-κB regulation does not require
234 IκBα at this stage or it might be compensated by the other IκBs (IκBβ, IκBε or p100), as
235 previously demonstrated [40,41]. This observation suggests that either NF-κB signaling is not
236 active in naïve pluripotency, which is supported by the low expression levels of NF-κB
237 subunits (see Figures 1B-C and 1E-F), or IκBα function on NF-κB is compensated by the other
238 IκBs (IκBβ, IκBε or p100), as previously demonstrated[40,41].

239 To further investigate the relative impact of both IκBα functions in mESCs, we took advantage
240 of recent results from our group that led to the identification of the specific IκBα protein
241 residues that define NF-κB- or chromatin-binding through H2A/H4. Mutation of these
242 residues allowed the generation of doxycycline-inducible (i) separation-of-function IκBα
243 mutants that are specifically deficient in one or the other function, at least in the intestinal
244 epithelial cells[32]. We called i-IκBα$^{\Delta Chromatin}$ the i-SOF IκBα mutant that interacts with NF-κB
245 but is deficient for H2A and H4 binding and i-IκBα$^{\Delta NF\text{-}\kappa B}$ the one that interact with histones but
246 is deficient for NF-κB subunits binding (Figure 5B and [32]). The three different IκBα forms (i-
247 IκBα^{WT}, i-IκBα$^{\Delta NF\text{-}\kappa B}$ and i-IκBα$^{\Delta Chromatin}$) were stably transfected in the IκBα KO mESCs and
248 induced by 16h of doxycycline treatment (Figure S4A). We used these cells to investigate the
249 biochemical properties and functional impact of SOF IκBα mutants in mESCs. By pull-down

250 experiments, we found that i-IκBα$^{\Delta NF\text{-}\kappa B}$ expressed in ESCs was able to interact with histone
251 H2A but not with the NF-κB member p50. In contrast, i-IκBα$^{\Delta Chromatin}$ interacts with p50 but
252 not with H2A, while i-IκBα^{WT} preserves both binding capacities (Figure 5C). In concordance
253 with these results, i-IκBα^{WT} and i-IκBα$^{\Delta NF\text{-}\kappa B}$ were found in both the cytoplasmic and chromatin
254 fractions of mESCs, whereas IκBα$^{\Delta Cromatin}$ was retained in the cytoplasm (Figures 5D-E). In
255 multiple experiments, we noticed a significant reduction in protein levels of IκBα$^{\Delta chromatin}$
256 despite the mRNA expression levels of the different IκBα forms being comparable (Figures 5C-
257 D and S4A).

258 Then, we studied whether i-IκBα^{WT} and/or the i-SOF IκBα mutants (IκBα$^{\Delta NF\text{-}\kappa B}$ or IκBα$^{\Delta Chromatin}$)
259 were able to reverse any of the phenotypes observed in the IκBα-KO mESCs (Figure S4B).
260 Induction of i-IκBα^{WT} and i-IκBα$^{\Delta NF\text{-}\kappa B}$ reduced the expression levels of the naïve pluripotent
261 genes *Zfp42, Klf2, Sox2* and *Tbx3*, which were increased by i-IκBα$^{\Delta Chromatin}$ (Figure 5F). In
262 addition, the ground state-associated DNA hypomethylation was specifically reverted in i-
263 IκBα^{WT} and i-IκBα$^{\Delta NF\text{-}\kappa B}$ mESCs but not in i-IκBα$^{\Delta Chromatin}$ mESCs (Figure 5G). Finally, we
264 addressed whether i-IκBα^{WT}, i-IκBα$^{\Delta NF\text{-}\kappa B}$ and i-IκBα$^{\Delta Chromatin}$ mESCs were capable to revert the
265 differentiation blockage of IκBα-KO ESCs (Figure S4B). Induction of IκBα^{WT} and IκBα$^{\Delta NF\text{-}\kappa B}$ was
266 enough to restore the differentiation potential of IκBα-KO mESCs into EBs, as indicated the
267 increase in the number of differentiated cells (based on percentage of SSEA-1^{neg} cells) (Figures
268 5H and S4C) and the reduced number of AP+ colonies (in the 216h IκBα-KO reconstituted EB
269 assays), which was similar to the number of colonies obtained from IκBαWT EBs (Figures 5I).
270 Lastly, the number of remaining pluripotent-like cells (defined by OCT3/4 NANOG staining)
271 was also reduced in i-IκBα^{WT} and i-IκBα$^{\Delta NF\text{-}\kappa B}$ 216h EBs, and only small and few regions of
272 undifferentiated cells was observed. In contrast, induction of i-IκBα$^{\Delta Chromatin}$ did not restore
273 the differentiation potential of IκBα-KO mESCs (Figures 5J and S4D).

274 These results demonstrate that the chromatin-dependent IκBα function, but not its NF-κB-
275 related activity, is necessary for the proper regulation of chromatin marks at specific genomic
276 regions that are linked to transcriptional changes that are likely at the base of the capacity of
277 ESCs to exit the ground state of naïve pluripotency and differentiate.

DISCUSSION

Here we have identified a new and unexpected function for the IκBα protein in the regulation of the naïve pluripotency exit. Using mESCs to investigate the role of IκBα in pluripotency maintenance and differentiation, we discovered that the absence of IκBα severely impairs the exit of pluripotency. Furthermore, IκBα-KO mESCs stabilizes the ground state of naïve pluripotency under Serum/LIF conditions, shedding light on its function as a critical regulator of the transition from naïve to primed pluripotency. While IκBα is commonly known for its role as an inhibitor of the NF-κB signaling pathway [26], our laboratory has previously furnished compelling evidence of its alternative role through its interaction with histones and other chromatin components [27,29,31]. We have demonstrated that chromatin-bound IκBα plays a crucial role in regulating skin and intestinal stem cells [27,28], hematopoietic stem cell development [42], and it influences the regenerative capacity of these tissues, and in some cases, their susceptibility to neoplastic transformation. Disentangling the chromatin-related function of IκBα from its canonical role as an inhibitor of NF-κB has been challenging, making it difficult to determine its truly biological significance. To tackle this challenge, we engineered separation-of-function (SOF) mutants of IκBα, as detailed in [43], by identifying specific residues that are essential for binding either NF-κB elements or histones. Interestingly, we have shown that only the histone-binding proficient IκBα mutant (IκBα$^{\Delta NF\text{-}\kappa B}$), which lacks the ability to bind to NF-κB, has the capability to reverse the stabilization of the ground state observed in IκBα-KO mESCs. This is sufficient to facilitate their exit from the state of naïve pluripotency, restoring their full differentiation potential (Figure 5). The involvement of NF-κB in pluripotency has been a subject of prior investigation. Studies have revealed that pluripotent cells display a dampened inflammatory signaling pathway, which is induced upon pluripotency dissolution and activation of differentiation [24,44]. However, the precise molecular mechanisms underlying the attenuated status of NF-κB during this stage remain incompletely understood. A recent work has shed light on a potential regulatory axis involving ATG5-β-TrCP1-NF-κB, proposing it as a mechanism that diminishes NF-κB activity by stabilizing the IκBα protein in mESCs [23]. In any case, since modification of canonical NF-κB activity directly impacts on the levels IκBα expression, the previous NF-κB-associated phenotypes should be reevaluated considering this chromatin role of IκBα. Furthermore, the expression of IκBα$^{\Delta Chromatin}$, which retains the inhibitory function of NF-κB, failed to mitigate the ground state stabilization observed in IκBα-KO mESCs (Figure 5). This finding suggests that the observed role of IκBα in regulating the exit from naïve pluripotency is not due to NF-κB inhibition. In fact, there is evidence that the chromatin function of IκBα is an ancestral function preceding its role as NF-κB inhibitor. In Caenorhabditis Elegans (*C.elegans*), which lacks NF-κB orthologs but possesses two homologs of IκBα, the absence of IκBα orthologs has severe multi-organ differentiation defects [39]. This observation further supports the notion that the chromatin-related function of IκBα plays a fundamental role in developmental processes, independent of its canonical role in NF-κB signaling.

317 We have observed that IκBα-KO mESCs exhibit epigenetic and transcriptomic profiles
318 resembling the ground state of naïve pluripotency under Serum/LIF culture (Figure 3). In this
319 regard, the fact that IκBα is preferentially located in the chromatin of mESCs cultured in
320 Serum/LIF, when they exhibit a high degree of heterogeneity, suggests that IκBα might act as
321 a regulator of this heterogeneity. One potential explanation might be that IκBα could be
322 affecting the stability of fluctuating transcription factors, which is crucial to mediate the
323 pluripotent-to-differentiation balance [3]. Thus, the lack of IκBα might stabilize those
324 transcription factors that would favor the ground-state observed in IκBα-KO mESCs cultured
325 in Serum/LIF. Further experiments are required to demonstrate this hypothesis. Moreover,
326 the differences in murine and human pluripotency [11] point out the necessity to address the
327 real impact of IκBα modulation in the stabilization of the ground state in human pluripotent
328 stem cells.

329 In summary, our work establishes that IκBα mediates the exit from naïve pluripotency by
330 modulating the activation of naïve pluripotency genes. Importantly, this newly identified role
331 of IκBα operates independently of its canonical function in inhibiting the NF-κB pathway. Our
332 findings underscore the intricate interplay between inflammation and pluripotency status,
333 revealing a previously unrecognized complexity in their interaction.

334 **METHODS**

335 **Cell culture**

336 mESC line ES-E14TG2a (ATCC; Cat #CRL-1821) was cultured on plastic dishes precoated with
337 0.1% (w/v) Gelatin (Sigma; Cat #G2500-100G) in Serum/LIF medium. Serum/LIF is composed
338 by DMEM basal medium (Sigma-Aldrich; Cat #D5796) supplemented with 15% FBS (ESC-
339 qualified; Gibco Cat #26140079), 1X Glutamax (Gibco; Cat #35050061), 1X NEAA (Gibco;
340 Cat#11140050), 1mM Sodium Pyruvate (Gibco; Cat#11360070), 1000U/mL Leukemia
341 Inhibitory Factor (LIF) (Millipore, Cat #ESG1107) and 0.125mM 2-mercaptoethanol (Gibco;
342 Cat#31350010). Medium was changed every day, and cells were splitted every other day using
343 TrypLE Express (Gibco; Cat #12605010) for harvesting. Cells were maintained in a 5% CO2
344 incubator at 37°C.

345 For inducing the ground-state of naïve pluripotency, mESCs were cultured in 2i/LIF medium
346 for 2 consecutive passages. 2i/LIF medium is composed by NDiff 227 medium (TAKARA, Cat
347 #Y40002) supplemented with 1000U/mL LIF, 0.4 µM PD032591 (Selleck Chemicals, Cat
348 #S1036) and 3 µM CHIR99021 (Merck, Cat #SML1046).

349 **Epiblast stem cell differentiation**

350 Differentiation from mESCs towards Epiblast Stem Cells (EpiSCs) was performed as previously
351 described [45]. $3x10^4$ mESCs were seeded in 6-well plastic dishes, and they were cultured in
352 Serum/LIF medium for 24h. Medium was then switched to NDiff 227 medium (TAKARA, Cat
353 #Y40002) supplemented with 20 ng/ml activin A (Cat. #120-14E; PeproTech) and 10 ng/ml Fgf
354 basic (R&D Systems, Cat #233-FB-025/CF). Cells were submitted to daily media changes till
355 day 5 (120h), when they were further analyzed.

356 **Embryoid bodies differentiation from mESCs**

357 Embryoid bodies differentiation was established as described in [46]. Briefly, mESCs were
358 splitted twice in Serum/LIF medium before inducing differentiation. Once mESCs are 80%
359 confluent, cells were collected using TrypLE Express. One well of 6-well plate was splitted in
360 an entire 6-well plate in IMDM-ES medium for 48h. IMDM-ES medium is composed of Iscove's
361 Modified Dulbecco's Medium (IMDM) (Cytiva, Cat #16SH30259.01) supplemented with 20%
362 FBS (ESC-qualified; Gibco Cat #26140079), 1X Glutamax (Gibco; Cat #35050061), 1X NEAA
363 (Gibco; Cat#11140050), 1mM Sodium Pyruvate (Gibco; Cat#11360070), 10ng/mL Leukemia
364 Inhibitory Factor (LIF) (Millipore, Cat #ESG1107) and 0.125mM 2-mercaptoethanol (Gibco;
365 Cat#31350010). For embryoid body induction, mESCs were harvested, and they were rinsed
366 twice with DPBS (Gibco; Cat #14190144). Cells were very well disaggregated into single-cells,
367 and 1.2 x 10^4 cells/mL embryoid body differentiation (EB^{diff}) medium were resuspended to a
368 total volume of 25mL of EB^{diff} medium. EB^{diff} medium is composed by IMDM supplemented
369 with 15% FBS (ESC-qualified; Gibco Cat #26140079), 1X Glutamax (Gibco; Cat #35050061), 50

370 µg/mL ascorbic acid (Sigma; Cat #A-4544), 180 µg/mL Transferrin (Roche; Cat #10652202001)
371 and 0.45 mM alpha-monothioglycerol (MTG) (Sigma; Cat #M6145). EBs were formed in
372 suspension for 5 days (120h). At day 5, in order to elongate the differentiation up to 216h
373 (day 9), EB^{diff} medium was refreshed by harvesting EBs with 10mL serological pipette,
374 centrifuge at 200 g for 3 min and EBs were resuspended in fresh EB^{diff} medium for 4 more
375 days.

376 **CRISPR/Cas9 gene editing and cell lines generation in mESCs**

377 The two guide RNAs (gRNAs) targeting the Nfkbia locus were designed using the CRISPR design
378 tool from MIT (http://crispr.mit.edu). The best 2 gRNAs (based on on-target and off-target
379 scores) that were targeting the exon 1 of Nfkbia (IκBα gene) were selected. After annealing,
380 one of the gRNAs was cloned into SpCas9(BB)-2A-GFP (px458) plasmid (Addgene; Cat #48138),
381 and the other gRNA was cloned into the px330-mCherry plasmid (modified from Addgene;
382 Cat #98750 to incorporate mCherry reporter). mESCs were co-transfected with the two
383 plasmids (px458-gRNA1 and px330-mCherry-gRNA2). $3x10^5$ cells were seeded a day before
384 per well of 6-well plate. At day of transfection, cells were washed once with 1X DPBS (Gibco;
385 Cat #14190144), and 2mL Opti-MEM medium (Gibco; Cat #31985070) was added into cells.
386 1.25 µg of each plasmid (2.5 µg of total DNA) was incubated with 10 µL of Lipofectamine 2000
387 (Invitrogen; Cat #11668019) in 240 µL of Opti-MEM for 20 min.
388 OptiMEM::Lipofectamine::DNA mixture was added into mESCs, and cells were incubated for
389 5 hours. Cells were then washed with DPBS, and medium was replaced by Serum/LIF. 48h
390 after transfection, GFP^+ $mCherry^+$ single cells were sorted by FACS using BD FACSAria II Cell
391 Sorter (BD Bioscience). Mutant clones were screened through PCR and western blotting to
392 identify single clones with no IκBα protein expression. Non-targeting scrambled gRNAs were
393 cloned into px458 and px330-mCherry plasmids as wildtype clones. Three independent clones
394 from each genotype (IκBα-WT and IκBα-KO) were selected for further experiments.

395 Doxycycline-inducible IκBα ($IκBα^{WT}$, $IκBα^{ΔNF-κB}$ and i-$IκBα^{ΔH2A/H4}$) mESCs were generated by
396 cloning the three different IκBα versions into a PiggyBac transposon system [47]. IκBα protein-
397 coding cDNAs were PCR-amplified, and NheI and SalI restriction sites were placed at the 5'
398 and 3' ends, respectively. T2A-EGFP fragment was amplified from PX458 plasmid, and SalI and
399 AgeI restriction sites were introduced at its 5' and 3' ends. PB-TRE backbone (Addgene, Cat#
400 63800) was digested with NheI and AgeI enzymes, and mNfkbia and T2A-EGFP fragments
401 were ligated into the PB-TRE digested vector. To generate mESCs containing the inducible
402 vector, IκBα-KO mESCs were co-transfected with PB-TRE-mNfkbia-T2A-EGFP and PiggyBac
403 transposase plasmids, and pool of transfected cells was selected by Hygromycin (100µg/mL)
404 for 7 days. Cells were doubly screened by FACS sorting green fluorescent protein after 24h of
405 doxycycline (1µg/mL) treatment. Pool of cells were used for further experiments. Oligos
406 sequences are included in supplementary table 1.

407 **Teratoma formation assay**

408 IκBα-WT and IκBα-KO mESCs grown in Serum/LIF (5×10^5) were injected intramuscularly into
409 severe combined immunodeficient mice (NSG). In order to favor 3D aggregation of cells and
410 teratoma formation, cells were resuspended in Matrigel Matrix (BD; Cat #356234) prior to
411 injection. Six weeks later, mice with tumors were euthanized, and tumors were fixed in
412 formaldehyde, embedded in paraffin, sectioned and stained with hematoxylin and eosin for
413 histological analysis.

414 **Immunofluorescence staining**

415 For immunostaining of mESCs, cells were seeded on 0.1% gelatin-coated coverslips on 6-well
416 plates; for EB immunofluorescence, they were collected directly from the plate. Samples were
417 washed twice with 1X PBS, and they were fixed at 4ºC for 30 minutes with 4% PFA (Electron
418 Microscopy Sciences; Cat #15713S). For immunofluorescence of 5-Methylcytosine (5mC),
419 fixed cells were incubated with 2M Hydrochloric Acid (Sigma-Aldrich, Cat #H1758) for 20
420 minutes at room temperature. Samples were then washed twice with 1X Tris-buffered saline
421 (TBS; 50 mM Tris-Cl, pH 8) and permeabilized and blocked with 1X TBS supplemented with 1%
422 Triton-X100 (MERCK; Cat #9036-19-5) and 6% FBS (Biological Industries; Cat #04-001-1A) for
423 2h at 4ºC. Samples were washed twice with 1X TBS supplemented with 6% FBS. Primary
424 antibody incubation was performed in 1X TBS plus 6% FBS and 0.3% or 0.5% Triton-X100 (0.3%
425 for 2D culture and 0.5% for EBs) overnight at 4ºC. The following primary antibodies were used:
426 OCT3/4 (1:250; Santa Cruz; Cat #sc-5279), NANOG (1:250; Novus Biologicals; Cat #NB100-
427 588), 5-Methylcytosine (1:500, Invitrogen, Cat #MA5-24694), H3K27Ac (1:2000, Abcam, Cat
428 #AB4729). Samples were then washed 4 times with 1X TBS, 5 min each washing. Secondary
429 antibody incubation was performed in TBS 1X plus 1% BSA (Sigma-Aldrich; Cat #9048-46-8)
430 for 2h at room temperature. The following antibodies were used: Alexa Fluor 488 donkey anti-
431 mouse antibody (1:1000; Invitrogen; Cat #A-21202), Alexa Fluor 647 donkey anti-mouse
432 antibody (1:1000; Invitrogen; Cat #A-31571), Alexa Fluor 594 donkey anti-rabbit antibody
433 (1:1000; Life Technologies; Cat #A-21207), Alexa Fluor 647 donkey anti-rabbit
434 antibody(1:1000, Invitrogen; Cat #A-31573). Samples were washed three times with 1X TBS
435 for 5 min at room temperature each rinse. Samples were mounted using DAPI Fluoromount-
436 G (Southern Biotech; Cat #0100-20).

437 **Microscopy and image acquisition**

438 Fluorescence images were acquired using Confocal Leica TCS SP5 (Leica Microsystems), and
439 Leica application software LAS AF (Leica Microsystems) was used to visualize the images.
440 Images of teratoma haematoxylin and eosin and immunohistochemistry stainings were
441 acquired using BX61 Olympus Microscope (Olympus), and PRECiV™ 2D Image and
442 Measurement Software (Olympus) was used to visualize the images. The Image J (version
443 1.15) was used for further analysis [48].

444 **Flow cytometry sample preparation and analysis**

445 Cells were collected and they were purified based on FACS using BD FACSAria II Cell Sorter
446 (BD Bioscience). Cells were sorted at 3,500 events/second, and at maximum flow rate of 4
447 and 85 µm nozzle. 5 µg/ml of DAPI (Biotium; Cat #BT-40043) was used as a viability dye. For
448 flow cytometry analysis of pluripotency exit, cells were disaggregated using TrypLE Express,
449 and they were incubated at 4ºC for 20 minutes with SSEA1-eFluor 660 Monoclonal Antibody
450 (1:200, Invitrogene, Cat #50-8813-42). BD LSRFortessa Cell Analyzer or BD LSR II Flow
451 Cytometer (BD Bioscience) were used for Flow Cytometry Analysis experiments. Flow
452 cytometry data were analyzed using FlowJo X v10.0.7 (BD Biosciences).

453 **RNA isolation, cDNA synthesis and quantitative RT-PCR**

454 Total RNA isolation from cells was performed using the RNeasy Plus Mini Kit (Qiagen; Cat
455 #74136) or RNeasy Micro Kit (Qiagen; Cat #74004) following manufacturer's instructions.
456 Amount of RNA was quantified with Nanodrop (Thermo Fisher; Cat #ND2000CLAPTOP), and
457 2 µg of total RNA was retro-transcribed using Transcriptor First Strand cDNA Synthesis Kit
458 (Roche; Cat #04897030001) following the manufacturer's instructions.

459 Quantitative RT-PCR was performed in triplicates for each sample, and SYBR Green I Master
460 Kit (Roche; Cat #04887352001) was used to carry out the reaction. qRT-PCR was performed
461 using the LightCycler 480 system (Roche). Relative expression levels were calculated as $2^{-\Delta CT}$
462 normalized with the average CT of the housekeeping gene Tbp or Gapdh. Oligos sequences
463 are found in supplementary table 1.

464 **Chromatin Immunoprecipitation (ChIP)**

465 4-6x10^7 mESCs were cross-linked by incubating them in DPBS (Gibco, Cat #14190094)
466 supplemented with 1% formaldehyde (Sigma-Aldrich; Cat #252549) for 10 min rocking at
467 room temperature. Cross-linking was stopped using 125 mM Glycine (Sigma-Aldrich, Cat
468 #G8790) rocking for 5 minutes at room temperature. Fixed cells were then washed twice with
469 ice-cold DPBS, and scrapped and collected using DPBS supplemented with
470 protease/phosphatase inhibitor cocktail composed by 1X cOmplete™, EDTA-free Protease
471 Inhibitor Cocktail (Roche, Cat #11873580001), 1 mM PMSF, 1mM Sodium Ortovanadate and
472 20 mM β-Glycerol phosphate. Cells were centrifuged at 3200g for 5 minutes at 4ºC. Cells were
473 lysed by resuspending cell pellet in ice-cold ChIP buffer (1 volume of SDS buffer [100mM NaCl,
474 50mM Tris-HCl pH 8.1, 5mM EDTA pH 8, 0.5% SDS] and 0.5 volume of triton dilution buffer
475 [100mM Tris-HCl pH 8.6, 100mM NaCl, 5mM EDTA pH 8, 5% Triton X-100]) supplemented with
476 protease/phosphatase inhibitor cocktail, and samples were sonicated using sonication beads
477 (Diagenode; Cat #C01020031) and the Bioruptor Pico Sonicator (Diagenode; Cat #B01060010)
478 for 20 cycles (each cycle 30 seconds on/30 seconds off) or till DNA fragments have 100-300bp
479 size. Samples were centrifuged at 16000g for 20 minutes at 4ºC. Chromatin was quantified,
480 and 30 µg of chromatin was incubated with every 5µg of antibody rotating for 16 hours (or
481 overnight) at 4ºC. The following antibodies were used: H3K4me3 (Abcam, Cat #ab8580),

482 H3K27me3 (Millipore, Cat ##07-449), H3K27Ac (Abcam, Cat #ab4729), H3K4me1 (Abcam, Cat
483 #ab8895). Samples were pulled down by incubation with Protein A-Sepharose™ CL-4B
484 (previously hydrated and blocked with 0.05% BSA) for 3h at 4ºC in rotation. Sample was
485 washed with a low salt washing buffer (50mM HEPES pH 7.5, 140mM NaCl and 1% Triton)
486 three times, one wash with a high salt wash buffer (50mM HEPES pH 7.5, 500mM NaCl and
487 1% Triton) and one wash with TE pH 8 (10mM Tris-HCl pH8, 1mM EDTA). Samples were then
488 eluted in 1% SDS and 100mM $NaHCO_3$. Samples were descrosslinked by incubating for 16
489 hours (or overnight) at 65ºC shaking at 450 rpm, and were treated with Proteinase K for 1h at
490 45ºC. DNA was purified using QIAquick PCR Purification Kit (Qiagen, Cat #28106), following
491 the manufacturer's instructions.

492 For ChIP followed by sequencing (ChIP-seq) Purified DNA concentration and integrity were
493 determined using Agilent Bioanalyzer (Agilent Technologies; Cat #G2939BA). Libraries were
494 prepared using standard protocols. Chromatin was sequenced using Illumina HiSeq platform
495 (Illumina, Inc.) (50bp single-end reads). Samples sequencing depth range was the following:
496 (i) H3K4me3: 2.56-2.74x10^7 reads, (ii) H3K27me3: 6.19-7.2x10^7 reads, (iii) H3K27Ac: 9.11-
497 10.65x10^7 reads and (iv) H3K4me1: 9.76-10.58x10^7 reads.

498 **ChIP-seq data analysis**

499 Quality control was performed on raw data with FASTQC tool. Raw reads were trimmed to
500 remove adapters presence with Trimgalore (v0.6.6) [49]. Default parameters were used except
501 for a minimum quality of 15 (Phred score) and an adapter removal stringency of 3bp overlap.
502 For H3K4me3, H3K27me3 and H3K4me1 data, trimmed reads were aligned to the reference
503 genome with Bowtie2 (v2.4.4) which was executed with default parameters [50]. Required
504 genome index was built with corresponding GRCm38 fasta file retrieved from Ensembl
505 (http://ftp.ensembl.org/pub/release-102/). Multimapped reads and those exhibiting MAPQ <
506 20 were removed. Randomly placed multi mappers were removed from the mapped reads.
507 For all cases, duplicated reads were marked with SAMtools (v1.15) [51]. Drosophila
508 Melanogaster spike-ins, present in H3K27me3, were discarded. NSC and RSC quality metrics
509 were computed with PhantomPeakQualTools (v1.2) [52]. ENCODE blacklisted regions (mm10
510 v2) were removed prior to peak calling. BigWig files were individually generated using
511 deepTools (v3.5.1) bamCoverage with -ignoreDuplicates -binSize 10 -smoothLength 30 -
512 effectiveGenomeSize 2308125349 -normalizeUsing RPGC and -extendReads
513 *Fragment_Length* options [53]. The effective genome size was particularized to a read length of
514 50bp and directly retrieved from deepTools web site
515 (https://deeptools.readthedocs.io/en/develop/content/feature/effectiveGenomeSize.html).
516 *Fragment_Length* was retrieved from PhantomPeakQualTools results. For all histone marks
517 except for H3K4me3, peak calling was conducted by means of epic2 (v0.0.52) with -effective-
518 genome-fraction 0.8452 -fragment-size *Fragment_Length* options and chromosome sizes
519 only referring to canonical chromosomes [54]. For H3K4me3, MACS2 (v2.2.7.1) was used to
520 identify peaks with -nomodel -extsize *Fragment_Length* -g 2308125349 options [55]. The

521 corresponding input sample was used in all peak calling computations. For the histone marks,
522 peaks were called with adjusted p-values (FDR) < 0.05.

523 Peak annotation was performed with ChIPseeker R (v4.2.1) package (v1.34.1) considering a
524 TSS region range between 5000 bp upstream and 100 bp downstream (Yu et al., 2015).
525 Required TxDb object was generated from the Ensembl GRCm38 gtf file retrieved
526 (http://ftp.ensembl.org/pub/release-102/). A consensus peakset was obtained from the
527 three biological replicates per histone mark and condition (IκBα-WT or IκBα-KO) by identifying
528 overlapping peaks in at least two out of the three replicates.

529 Differential binding analysis (DBA) was conducted with DiffBind (v3.8.4) per histone mark [56].
530 Default parameters were used except for the summits parameter which was set to 500bp for
531 all histone marks except for H3K4me3 (150bp) in order to consider, for testing, intervals of
532 1000bp or 300bp respectively. Summit values were selected to have interval widths between
533 the minimum and first quartile peak width values for each histone mark. EdgeR was the
534 statistical method used for all the three analyses. Differentially bound regions (DBRs)
535 between IκBα-KO and IκBα-WT samples were called with adjusted p-values (FDR) < 0.05.
536 Identified DBRs with any annotated gene were plotted with EnrichedHeatmap R package
537 (v1.18.1) [57]. To summarize replicates per condition, normalizeToMatrix function was used
538 based on corresponding BigWig files in w0 mean mode in 50bp windows. Tracks visualization
539 were obtained by means of Integrative Genomics Browser (IGV) tool [58].

540 **Enhancers activity identification**

541 Consensus peaksets derived from the three H3K27ac and H3K4me1 IκBα-WT mESCs replicates
542 were used to identify poised and active enhancers in an IκBα-WT scenario. Putative poised
543 enhancers were defined as those regions with H3K4me1 but no H3K27ac peaks. Putative
544 active enhancers were defined as those regions with H3K27ac and presence/absence
545 H3K4me1 peaks. To assess any differential enhancers activity in IκBα-KO vs IκBα-WT mESCs
546 cultured in Serum/LIF, differentially bound regions and consensus peaksets (IκBα-KO)
547 identified in H3K4me1 and H3K27ac were required. Putative gained or lost poised/active
548 enhancers in IκBα $^{-/-}$ were obtained with following criteria: (i) for gained/lost poised enhancers
549 in IκBα $^{-/-}$: a differential H3K4me1 increase/decrease and absence of H3K27ac peaks in IκBα $^{-/-}$
550 consensus peakset, (ii) for gained/lost active enhancers (without H3K4me1) in IκBα-KO: a
551 differential H3K27ac increase/decrease and absence of H3K4me1 in IκBα-KO consensus
552 peakset and (iii) for gained/lost active enhancers (with H3K4me1) in IκBα-KO: a differential
553 H3K27ac increase/decrease and presence of H3K4me1 in IκBα $^{-/-}$ consensus peakset.

554 A maximum gap of 1000bp was allowed for checking the overlap between two different
555 histone marks. For this purpose, the 'subsetByOverlaps' function from the IRanges R package
556 was used (v.2.34.1).

557 **RNA-seq experiments**

558 Total RNA from three independent clones from mESCs, 48h EBs and 96h EBs was isolated
559 using the RNeasy Plus Mini Kit (Qiagen; Cat #74136) following manufacturer's instructions.
560 Amount of RNA was quantified with Nanodrop (Thermo Fisher; Cat #ND2000CLAPTOP), and
561 RNA integrity was addressed by agarose gel and Agilent Bioanalyzer (Agilent Technologies;
562 Cat #G2939BA). Libraries sequenced using Illumina HiSeq 2500 (Illumina, Inc.) (125bp paired-
563 end reads). Samples sequencing depth ranged between 35M and 52M reads (average 41M
564 reads) per sample.

565 **RNA-seq data analysis**

566 Quality control was performed on raw data with the FASTQC tool (v0.11.9). Raw reads were
567 trimmed to remove adapter presence with Trimgalore (v0.6.6) [49]. Default parameters were
568 used except for a minimum quality of 15 (Phred score) and an adapter removal stringency of
569 3bp overlap. Trimmed reads were aligned to reference the genome with STAR aligner tool
570 (v2.7.8). STAR was executed with default parameters except for the number of allowed
571 mismatches which was set to 1. Required genome index was built with corresponding
572 GRCm38 gtf and fasta files retrieved from Ensembl (http://ftp.ensembl.org/pub/release-
573 102/). Obtained BAM files with uniquely mapped reads were considered for further analysis.
574 Raw gene expression was quantified using featureCounts tool from subRead software (v2.0.1)
575 with exon as feature [59]. The raw counts matrix was imported into the R Statistical Software
576 environment (v4.2.1) for downstream analysis. Raw expression matrix included 55,487 genes
577 per 18 samples in total. Experimental design considered three timepoints: mouse ESCs, EBs
578 at 48h and EBs at 96h. Each time point included 6 samples distributed in two conditions: 3
579 IκBα-WT and 3 IκBα-KO. Prior to statistical analysis, those genes with less than 10 raw counts
580 across the 6 samples under test were removed. After pre-filtering, 21,843 genes (mESCs),
581 21,424 genes (EBs 48h) or 21,664 genes (EBs 96h) were available for testing. For visualization
582 purposes, counts were normalized by the variance-stabilizing transformation method as
583 implemented in DESeq2 R package [60] (v1.38.3). Differential expression analysis (DEA) was
584 conducted with DESeq2. Each time point was independently analyzed. Fitted statistical model
585 included sample conditions as covariable with IκBα-WT as the reference. Obtained log2 fold
586 change values were shrunken with apeglm shrinkage estimator R package (v1.20.0) [61]. Raw p-
587 values were adjusted for multiple testing using the Benjamini-Hochberg False Discovery Rate
588 (FDR) [62]. Differentially Expressed Genes (DEGs) between IκBα-KO and IκBα-WT samples were
589 called with adjusted p-values (FDR) < 0.05 and absolute shrunken log2 Fold change > 1. Data
590 visualization was performed with the ggplot2 (v3.4.1).

591 **Genome-wide DNA methylation samples preparation**

592 DNA from frozen mESCs pellets was extracted using DNeasy Blood and Tissue Kit (Qiagen
593 GmbH, Hilden, Germany). Purified genomic DNA was quantified with Qubit (Invitrogen,
594 Carlsbad, CA, USA) according to manufacturer's instructions. Infinium Mouse Methylation
595 BeadChip (Illumina, Inc., San Diego, CA, USA) arrays were used to profile DNA methylation

596 genome wide. This platform allows over 285,000 methylation sites per sample to be
597 interrogated at single-nucleotide resolution. The samples were bisulfite converted using EZ
598 DNA Methylation-Gold™ Kit (Zymo Research, CA, USA) and were hybridized in the array
599 following the manufacturer's instructions.

600 **DNA methylation data analysis**

601 The DNA methylation profile of the studied samples was assessed using the Infinium Mouse
602 Methylation BeadChip Array (~285,000 methylation sites) as previously described [63]. Briefly,
603 raw signal intensities were obtained with GenomeStudio Software 2011.1 (Illumina) and DNA
604 methylation beta values were computed from raw IDAT files using GenomeStudio default
605 normalization with control probes and background subtraction. Quality control steps to
606 remove erratic probe signals were performed within the R statistical environment (v4.0.3).
607 We removed probes with detection p value > 0.01, genotyping probes and manufacturing
608 flagged (MFG) probes described in the Illumina manifest file
609 (https://support.illumina.com/downloads/infinium-mouse-methylation-manifest-file.html).
610 The differentially methylated probes (DMPs) between IκBα-WT and IκBα-KO samples were
611 computed separately for each time point (mESCs and EBs at 96h) by deriving a linear model
612 with the limma R package (v3.46.0). Each condition included 3 samples per time point. DMPs
613 with adjusted p-value (FDR) <0.05 and absolute mean methylation beta value difference
614 between conditions >0.3 were considered significant. DNA methylation analysis was
615 performed using the mm10 mouse genome reference build and the complete annotation was
616 downloaded from the annotated manifest file
617 (http://zwdzwd.github.io/InfiniumAnnotation#mouse) [36].

618 **Functional analysis**

619 Overrepresentation analysis was applied over lists of selected genes derived from RNA-seq
620 data (DEGs) or from ChIP-seq data (differentially bound regions). The Gene Ontology
621 (Biological Process ontology, GO BP terms), KEGG PATHWAY and WikiPathways databases for
622 Mus Musculus [64–66] were interrogated by means of clusterProfiler R package (v4.6.2) (Wu et
623 al., 2021). Corresponding Entrez identifiers were used. Benjamini-Hochberg procedure was
624 used to obtain adjusted p-values. Obtained GO BP terms were simplified using the simplify
625 function from clusterProfiler with default parameters. Overrepresented terms or processes
626 were called with adjusted p-values (FDR) < 0.05.

627 Gene Set Enrichment Analysis (GSEA) was performed for mESCs against the three cell states
628 signatures defined by other authors [67]. Briefly, each signature was composed of 200 genes
629 uniquely expressed in each state obtained from bulk RNA-seq performed per state. For this
630 purpose, the complete list of genes from mESCs samples (21,843 genes) was ranked based on
631 the shrunken log2 Fold Change obtained from DEA. GSEA was conducted through the

632 fgseaMultilevel function from fgsea R package (v1.24.0) [68] with default parameters.
633 Enrichment plots were generated with the same package.

634 Additionally, the testEnrichment function from SeSAMe R package (v1.14.2) [69] was used for
635 conducting functional analysis with default parameters over the list of DMPs. Probe design,
636 transcription factor binding site and histone modifications consensus database sets, included
637 in the same package, were interrogated.

638 Gene Set Variation Analysis (GSVA) R package (v1.46.0) with default parameters were used to
639 obtain Z-score values for genes annotated to endoderm (GO:0001706), mesoderm
640 (GO:0001707) and ectoderm (GO:0001705) GO BP terms [70].

641 **Statistical analysis**

642 Statistical analysis was performed with GraphPad Prism v.8.0.1. (GraphPad Software, Inc.).
643 Unless specified, the comparison between two groups was performed with unpaired two-
644 sided t-test. A p-value < 0.05 was considered significant.

645 **DATA AVAILABILITY**

646 All sequencing data is deposited at GEO under a SuperSeries with the accession number
647 GSE239565)[https://www.ncbi.nlm.nih.gov/geo/query/acc.cgi?acc=GSE239565]. Individual
648 SubSeries can be found at: GSE239563 (RNA-seq data), GSE239564 (ChIP-seq data) and
649 GSE239562 (Methylation array data).

650 **CODE AVAILABILITY**

651 Scripts used to process the generated bulk RNA-seq and ChIP-seq data are available in Github
652 repository: https://github.com/BigaSpinosaLab/PAPER_IkBa_Naive_Pluripotency

653 **ACKNOWLEDGEMENTS**

654 We would like to acknowledge all members of the Bigas/Espinosa labs for helpful discussions.
655 We are grateful for technical support to CRG/UPF Flow Cytometry Unit, CRG Genomics and
656 Advanced Light Microscopy Units. This work has been supported by Spanish Ministry of
657 Science and Innovation (PID2019-104695RB-I00, PLEC2021-007518, PDC2021-120817-I00),
658 Generalitat de Catalunya (2021SGR 39) and Departament de Salut (SLT002/16/00299) to AB;
659 the Spanish Ministry of Science and Innovation (PID2019-108322GB-100 and PID2022-
660 142679NB-I00) to LDC; the Spanish Ministry of Science and Innovation (PID2021-123383NB-
661 I00.) and the Agencia de Gestió d'Ajuts Universitaris i de Recerca (2021 SGR 01222) to BP.
662 L.G.P has been a recipient of FI AGAUR fellowship (2019 FI-B 00151/2020 FI_B1 00130) from
663 Generalitat de Catalunya. D.A-V was funded by the FIS fellowship (FI20/00130) from Instituto
664 Carlos III. M.B. received funding from the Ramón Areces Foundation. M.M. is a recipient of a
665 grant from the Instituto Carlos III, grant number CA22/00011 (co-funded by the European
666 Social Fund Plus, ESF+ and by the European Union).

667

668

669 **AUTHOR CONTRIBUTION**

670 L.G.P, L.E and A.B designed the study. L.G.P, D.A-V, M.B, A.I, J.G, J.B, D.A.E, C.A.G.P, C.B, V.R.C
671 and A.V performed experiments. L.G.P, M.M, M.B and C.A.G.P performed bioinformatics
672 analysis. L.G and A.B wrote the manuscript with input from all authors. C.B, A.V, A.V, P.M,

L.D.C, G.S, B.P, M.E and L.E provided input on experimental design. L.E and A.B provided resources and supervised the research.

675 **FIGURE LEGENDS**

676 **Figure 1. IκBα is highly expressed in pluripotent cells. A.** Schematic of pluripotent states in
677 mouse embryonic stem cells (mESCs). mESCs were maintained regularly in naïve pluripotency
678 by culturing them in serum/LIF medium, or they were polarized towards the ground state of
679 naïve pluripotency by culturing them for two passages in LIF plus Gsk3β (CHIR99021 or Chiron)
680 and MEK (PD0325091) inhibitors (2i/LIF). mESCs were further differentiated towards the
681 primed pluripotent state (epiblast-like cells) by culturing mESCs in a medium containing
682 20ng/mL Activin A and 10ng/mL Fgf2 for 120h. **B-C.** Relative mRNA levels (based on qPCR
683 experiments) of the canonical IκB genes (*Nfkbia, Nfkbib, Nfkbie*) (**B**) or Nf-κB effector genes
684 (*Rela, c-Rel, Relb, Nfkb1, Nfkb2*) (**C**) across the different states of pluripotency. Expression was
685 normalized using the house-keeping gene *Tbp* relative to 2i/LIF. Data from three independent
686 experiments. Dots indicate mean values and error bars refer to ± standard deviation (SD). **D.**
687 Western blot analysis of IκBα protein distribution in cytoplasm, nucleoplasm (Nucleus) or
688 chromatin in cells at the ground-state of naïve pluripotency (2i/L), naïve pluripotency (S/L) or
689 primed pluripotency (Epi). **E.** Transcriptome and proteome differences across naïve (2i/LIF)
690 and primed (Epiblast-like cells or EpiSCs) pluripotent states. Enriched transcripts and proteins
691 in naïve state are highlighted in red (Log_2 fold-change < -1). Enriched transcripts and proteins
692 in the primed state are marked in dark gray (Log_2 fold-change > 1). Data from [33]. **F.** Heatmap
693 showing the expression levels of pluripotency (*Dppa4, Pou5f1, Sox2, Prdm14, Klf4, Zfp42,*
694 *Nanog*), differentiation (*Mesp1, Gata4, Gata6, Lhx1, Wnt3a, Fgf5, Nes, Axin2, Wnt3, Eomes,*
695 *Foxa2, T, Mixl1, Lef1*) NF-κB (*Nfkbia, Nfkbib, Nfkbie, Nfkbiz, Rela, c-Rel, Relb*) and Polycomb
696 (*Ezh1, Ezh2, Eed, Epop, Jarid2, Suz12, Mtf2, Aebp2*) genes from the RNAseq samples at mESCs
697 (Serum/LIF) and differentiating cells (embryoid bodies) at 48h and 96h of IκBα-WT cells.
698 Normalized counts based on z-score are represented.

699 **Figure 2. The absence of IκBα hinders the exit from the pluripotent state and prevents the**
700 **activation of differentiation programs. A.** Representative immunofluorescence of 216h EBs
701 stained with the pluripotency markers NANOG and OCT3/4. **B.** Quantification of total number
702 of alkaline phosphatase (AP) colonies after 216h EB differentiation and additional culture of
703 96h in Serum/LIF (S/L) medium. Dots represent values from two independent experiments
704 from three different IκBα-WT or IκBα-KO clones. Unpaired two-sided t-test applied.
705 Representative images from AP colonies are included in the upper panel. **C.** PC1 and PC2 from
706 Principal Component Analysis (PCA) of normalized RNA-seq data from 3 different time points
707 (mESCs, 48h EBs and 96h EBs) of IκBα-WT and IκBα-KO cells (three independent clones from
708 each genotype). **D.** Heatmap showing the expression levels of naïve pluripotency genes
709 (*Gab1, Sox2, Esrrb, Zfp42, Dppa4, Klf2, Prdm14, Klf4, Tfcp2l1*) from the RNAseq samples of
710 IκBα-WT and IκBα-KO EBs at 96h. Normalized counts based on z-score are represented. **E-G**.
711 Z-score values for gene sets referring to Endoderm (E), Mesoderm (F) and Ectoderm (G)
712 formation from The Gene Ontology database (GO:0001706, GO:0001707 and GO:0001705
713 terms, respectively) and obtained from corresponding expression levels at mESCs, 48h and
714 96h EBs IκBα-WT or IκBα-KO cells (three independent clones of each genotype). Loess curves

715 are also represented with 95% confidence intervals (shadowed area surrounding the curves).
716 **H.** Schematic of teratoma formation assay. $5x10^5$ IκBα-WT or IκBα-KO mESCs cultured in
717 Serum/LIF were injected intramuscularly in the leg of immunocompromised NSG mice. 6
718 weeks after the transplant, teratomas were formed, and mice were euthanized for further
719 teratoma analysis. **I.** Representative images of immunohistochemistry for OCT3/4 in IκBα-WT
720 (left panel) or IκBα-KO (right panel) teratomas. Teratomas were derived from three
721 independent clones of mESCs of both genotypes. **J.** Percentage of $OCT3/4^+$ cells in teratomas.
722 Positive cells were counted from five different microscope fields from each IκBα-WT and IκBα-
723 KO clone. Unpaired two-sided t-test was performed. Bars indicate mean values and error bars
724 refer to ± SD.

725 **Figure 3. IκBα-KO mESCs retain the ground-state of naïve pluripotency under Serum/LIF**
726 **culture. A.** (Upper panel) Schematics of mESCs differentiation towards Epiblast Stem Cells
727 (EpiSCs). mESCs cultured in Serum/LIF were then seeded in N2B27 medium supplemented
728 with 10ng/mL Fgf2 and 20ng/mL Activin A for 120h (see Materials and Methods section for
729 further information). (Bottom panel) Relative RNA levels (based on qPCR experiments) of
730 naïve pluripotency genes (*Nanog, Sox2, Rex1, Klf4, Gbx2, Tbx3, Dppa3*) in IκBα-WT or IκBα-KO
731 EpiSCs at 120h. RNA levels were normalized based on *Tbp* expression relative to IκBα-WT.
732 Each dot represents an independent clone either from IκBα-WT or IκBα-KO genotypes.
733 Unpaired two-sided t-test applied. Horizontal bars indicate mean values and error bars refer
734 to ± SD. **B.** GSEA results comparing IκBα-KO vs IκBα-WT mESCs cultured in Serum/LIF against
735 ground (2i/LIF) and naïve (Serum/LIF) state pluripotency signatures retrieved from [35].
736 Adjusted p-value by Benjamini-Hochberg procedure and Normalized Enrichment Score (NES)
737 indicated. **C.** Relative RNA levels of the naïve pluripotency genes *Rex1 (Zfp42), Klf2* and *Tbx3*
738 upon culture of IκBα-WT either in Serum/LIF or two passages in 2i/LIF. 2i/LIF IκBα-WT mESCs
739 were compared with IκBα-KO mESCs cultured in Serum/LIF. Unpaired two-sided t-test was
740 applied to calculate statistical significance. Each dot represents an independent clone from
741 each of the two genotypes. **D.** Representative immunofluorescence images of DNA-
742 methylation-related mark 5-methylcytosine (5mC) in IκBα-WT (left) and IκBα-KO (right)
743 mESCs cultured in Serum/LIF. **E.** DNA methylation profile (using DNA methylation arrays [36]) in
744 IκBα-WT vs IκBα-KO mESCs (upper) and 96h EBs (bottom panel) showing the distribution
745 density of mean ß-values from all 261,220 CpGs under test per condition.

746 **Figure 4. Absence of IκBα reinforces the pluripotency program at the epigenetic and**
747 **transcriptional levels. A.** ChIP-seq Enrichment Analysis (ChEA) of differentially expressed
748 genes (DEGs; adjusted p-value<0.05) in IκBα-KO mESCs. P-value was calculated using Fisher
749 exact test. **B.** Number of differentially bound regions (adjusted p-value <0.05, FDR) for
750 H3K4me3 and H3K27me3 histone marks in IκBα $^{-/-}$ vs IκBα $^{+/+}$ mESCs cultured in Serum/LIF.
751 Enriched or reduced regions in IκBα $^{-/-}$ mESCs are distinguished (log_2 Fold-change >0 or <0,
752 respectively). Overrepresented WikiPathways, for (left) H3K4me3 and (right) H3K27me3 are
753 indicated. Annotated genes to differential regions showing H3K4me3 enrichment or
754 H3K27me3 reduction were considered. A one-sided hypergeometric test was conducted. **C.**

755 Venn Diagram of genes contained in regions with either increased H3K4me3 or reduced levels
756 of H3K27me3. Statistical significance of the overlapping was calculated using the chi-squared
757 method. Overrepresented pathways for genes containing increased H3K4me3 and reduced
758 H3K27me3 levels are indicated (only pathways with an adjusted p-value<0.05 were
759 considered). **D-E.** Representative genomic regions of naïve pluripotency genes having either
760 differential enriched H3K4me3-only (D) or reduced H3K27me3-only (E) levels in IκBα-KO vs
761 IκBα-WT mESCs cultured in Serum/LIF. Shadowed regions highlight the differential levels of
762 the histone marks. **F.** Number of regions with differential enhancer activity in IκBα-KO vs IκBα-
763 WT mESCs cultured in Serum/LIF. Increased/Reduced activity for (left) poised enhancers
764 based on the H3K4me1 differential binding and absence of H3K27ac overlapping peaks in
765 IκBα-KO mESCs and, (right) active enhancers based on the differential binding of H3K27ac
766 and presence of H3K4me1 overlapping peaks in IκBα-KO. Differential binding based on
767 adjusted p-value <0.05 (FDR). Increased or reduced regions in IκBα-KO are distinguished by
768 log_2 Fold-change >0 or <0, respectively, compared to IκBα-WT mESCs. Overrepresented
769 WikiPathways for annotated genes to (left) poised enhancers with reduced activity and (right)
770 active enhancers with increased activity in IκBα-KO vs IκBα-WT mESCs are indicated
771 (adjusted p-value < 0.05, FDR). A one-sided hypergeometric test was conducted. **G.**
772 Representative genomic regions of naïve pluripotency genes having an increase in active
773 enhancer status (H3K27Ac enrichment) in IκBα-KO mESCs cultured in Serum/LIF. Shadowed
774 regions highlight the differential levels of the histone mark. **H.** Heatmap showing the
775 expression levels of the naïve pluripotency genes from the RNAseq samples of IκBα-KO and
776 IκBα-WT mESCs cultured in Serum/LIF. Normalized counts (z-score) from genes are
777 represented.

778 **Figure 5. IκBα prevents the hyperactivation of naïve pluripotency program in an NF-κB-**
779 **independent manner. A.** Boxplots, violin plots and individual values representing the
780 normalized gene expression levels in IκBα-WT or IκBα-KO mESCs, EBs 48h and EBs 96h.
781 Considered genes are those annotated to NF-κB signaling pathway (KEGG PATHWAY
782 mmu04064). Box Plots: center line, median; lower and upper hinges, first and third quartiles;
783 whiskers, 1.5x interquartile range (IQR) extended to the largest/smallest value within 1.5xIQR;
784 no outliers present. Unpaired two-sided Wilcoxon test applied. **B.** Schematic of chromatin-
785 specific/NF-κB-deficient (IκBα$^{\Delta NF\text{-}\kappa B}$) or NF-κB-specific/chromatin-deficient (IκBα$^{\Delta Chrom}$) IκBα
786 mutants (Separation-Of-Function or SOF mutants). **C.** Pull-down of GST-H2A and GST-P50 with
787 cell lysates from different SOF IκBα mutant mESCs. **D.** Western blot analysis of cytoplasmic
788 protein extracts of doxycycline-inducible IκBα forms (i-IκBα$^{\Delta WT}$, i-IκBα$^{\Delta NF\text{-}\kappa B}$, i-IκBα$^{\Delta Chrom}$) after
789 16h of doxycycline induction. **E.** Western blot analysis of chromatin protein extracts of
790 doxycycline-inducible IκBα forms (i-IκBα$^{\Delta WT}$, i-IκBα$^{\Delta NF\text{-}\kappa B}$, IκBα$^{\Delta Chrom}$) after 16h of doxycycline
791 induction. **F.** Relative RNA levels of naïve pluripotency genes (*Zfp42, Klf2, Sox2, Tbx3*) in i-
792 IκBα^{WT}, i-IκBα$^{\Delta NF\text{-}\kappa B}$ and i-IκBα$^{\Delta Chrom}$ mESCs after doxycycline induction. Unpaired two-sided t-
793 test was performed. Bars indicate mean values and error bars refer to ± SEM. **G.**
794 Representative immunofluorescence images of DNA-methylation-related mark 5-

795 methylcytosine (5mC) in i-IκBα$^{\Delta WT}$ (upper panel), i-IκBα$^{\Delta NF\text{-}\kappa B}$ (medium panel), IκBα$^{\Delta Chrom}$
796 (bottom panel) mESCs cultured in Serum/LIF. **H.** Flow cytometry analysis of the pluripotency
797 surface marker SSEA-1 at 216h EBs in i-IκBα^{WT}, i-IκBα$^{\Delta NF\text{-}\kappa B}$ and i-IκBα$^{\Delta Chrom}$ cells. **I.**
798 Quantification of Alkaline Phosphatase (AP) staining in 216h EBs upon reconstitution with the
799 different IκBα forms. Each dot represents an independent experiment. One-way ANOVA was
800 applied. Bars indicate mean values and error bars refer to ± SEM. Representative images of
801 Alkaline Phosphatase (AP) staining in 216h EBs are included in the upper panel. **J.**
802 Representative immunofluorescence for NANOG and OCT3/4 at 216h EBs in i-IκBα^{WT} (upper
803 panel), i-IκBα$^{\Delta NF\text{-}\kappa B}$ (medium panel) and i-IκBα$^{\Delta Chrom}$ (bottom panel) cells.

804 **Figure S1. Depletion of IκBα in mESCs compromises the exit from pluripotency. Related to**
805 **Figure 2. A.** Schematic of the approach followed to deplete IκBα protein in mESCs (upper
806 panel) and western blot analysis of three independent IκBα-WT and IκBα-KO mESC clones
807 (bottom panel). **B.** Flow cytometry plots of SSEA-1 from IκBα-WT or IκBα-KO EBs 216h. **C.**
808 Relative RNA levels (based on qPCR experiments) of naïve pluripotency genes (*Pou5f1, Gbx2,*
809 *Klf2, Sox2, Rex1, Nanog*) in IκBα-WT or IκBα-KO 216h EBs. RNA levels were normalized based
810 on *Tbp* expression relative to IκBα-WT. Each dot represents an independent clone either from
811 IκBα-WT or IκBα-KO genotypes. Unpaired two-sided t-test was applied. **D.** Schematic of
812 Alkaline Phosphatase (AP) staining carried out in EBs. IκBα-WT or IκBα-KO 216h EBs were
813 dissociated and seeded in Serum/LIF medium for another 96h. Attached cells were screened
814 for AP^{+} total cell number. **E.** Violin plot and individual values showing the quantification of
815 relative size of 168h EBs. Each dot represents an embryoid body. Unpaired two-sided t-test
816 was applied. **F.** Volcano plot from differential expression analysis between IκBα-KO vs IκBα-
817 WT 96h EBs. Dashed vertical lines represent an absolute shrunken $\log_2$ Fold Change = 1 and
818 dashed horizontal line represents an adjusted p-value = 0.05 (FDR).

819 **Figure S2. Absence of IκBα favors the ground-state of naïve pluripotency in Serum/LIF**
820 **conditions. Related to Figure 3. A.** Brightfield images of IκBα-WT or IκBα-KO EpiSCs at 120h.
821 Each picture corresponds to an independent clone from either IκBα-WT or IκBα-KO
822 genotypes. **B.** Bright-field microscopy images of IκBα-WT and IκBα-KO mESCs cultured in
823 Serum/LIF conditions. Two independent clones from each genotype are shown. **C.** DNA
824 methylation levels (mean ß-values) across chromosomes in IκBα-WT vs IκBα-KO mESCs.

825 **Figure S3. Epigenetic rewiring characterization in IκBα-KO mESCs cultured in Serum/LIF.**
826 **Related to Figure 4. A-D.** Volcano plots from differential binding analysis of H3K4me3 (A),
827 H3K27me3 (B), H3K4me1 (C) and H3K27Ac (D) in IκBα-WT vs IκBα-KO mESCs cultured in
828 Serum/LIF. Representative genes with enriched or reduced levels of H3K4me3 (A), H3K27me3
829 (B), H3K4me1 (C) and H3K27Ac (D) marks in IκBα-KO mESCs are highlighted.

830 **Figure S4. Reversion of IκBα-KO-related hyper pluripotent status is NF-κB independent.**
831 **Related to Figure 5. A.** Relative expression level of Nfkbia gene after overnight doxycycline
832 induction in i-IκBα$^{\Delta WT}$, i-IκBα$^{\Delta NF\text{-}\kappa B}$ and IκBα$^{\Delta Chrom}$ mESCs. **B.** Schematic representation of

833 reconstitution of IκBα-KO mESCs with either of the two doxycycline-inducible SOF mutants (i-
834 IκBα$^{\Delta NF\text{-}\kappa B}$ or IκBα$^{\Delta Chrom}$). mESCs were then kept in Serum/LIF medium supplemented with
835 1µg/mL Doxycycline for 4 consecutive passages. mESCs were characterized at the pluripotent
836 level and then their potential to be further differentiated was addressed. **C.** Percentage of
837 differentiated cells (determined as SSEA-1.) at 216h EBs 216h derived from i-IκBα$^{\Delta WT}$, i-
838 IκBα$^{\Delta NF\text{-}\kappa B}$ and IκBα$^{\Delta Chrom}$ mESCs. **D.** Quantification of EB differentiation status (percentage of
839 pluripotent cells) at 216h after induction of SOF IκBα mutants. Data from three independent
840 experiments.

841 **REFERENCES**

842 1. Festuccia, N., Osorno, R., Wilson, V., and Chambers, I. (2013). The role of pluripotency
843 gene regulatory network components in mediating transitions between pluripotent cell
844 states. Curr. Opin. Genet. Dev. *23*, 504–511.

845 2. Graf, T., and Stadtfeld, M. (2008). Heterogeneity of embryonic and adult stem cells. Cell
846 Stem Cell *3*, 480–483.

847 3. Martinez Arias, A., and Brickman, J.M. (2011). Gene expression heterogeneities in
848 embryonic stem cell populations: origin and function. Curr. Opin. Cell Biol. *23*, 650–656.

849 4. Pera, M.F., and Rossant, J. (2021). The exploration of pluripotency space: Charting cell
850 state transitions in peri-implantation development. Cell Stem Cell *28*, 1896–1906.

851 5. Wang, X., and Wu, Q. (2022). The Divergent Pluripotent States in Mouse and Human
852 Cells. Genes *13*. 10.3390/genes13081459.

853 6. Ying, Q.-L., Wray, J., Nichols, J., Batlle-Morera, L., Doble, B., Woodgett, J., Cohen, P.,
854 and Smith, A. (2008). The ground state of embryonic stem cell self-renewal. Nature
855 *453*, 519–523.

856 7. Marks, H., Kalkan, T., Menafra, R., Denissov, S., Jones, K., Hofemeister, H., Nichols, J.,
857 Kranz, A., Stewart, A.F., Smith, A., et al. (2012). The transcriptional and epigenomic
858 foundations of ground state pluripotency. Cell *149*, 590–604.

859 8. Boroviak, T., Loos, R., Lombard, P., Okahara, J., Behr, R., Sasaki, E., Nichols, J., Smith, A.,
860 and Bertone, P. (2015). Lineage-Specific Profiling Delineates the Emergence and
861 Progression of Naive Pluripotency in Mammalian Embryogenesis. Dev. Cell *35*, 366–
862 382.

863 9. Brons, I.G.M., Smithers, L.E., Trotter, M.W.B., Rugg-Gunn, P., Sun, B., Chuva de Sousa
864 Lopes, S.M., Howlett, S.K., Clarkson, A., Ahrlund-Richter, L., Pedersen, R.A., et al.
865 (2007). Derivation of pluripotent epiblast stem cells from mammalian embryos. Nature
866 *448*, 191–195.

867 10. Tesar, P.J., Chenoweth, J.G., Brook, F.A., Davies, T.J., Evans, E.P., Mack, D.L., Gardner,
868 R.L., and McKay, R.D.G. (2007). New cell lines from mouse epiblast share defining
869 features with human embryonic stem cells. Nature *448*, 196–199.

870 11. Weinberger, L., Ayyash, M., Novershtern, N., and Hanna, J.H. (2016). Dynamic stem cell
871 states: naive to primed pluripotency in rodents and humans. Nat. Rev. Mol. Cell Biol.
872 *17*, 155–169.

873 12. Guo, G., Yang, J., Nichols, J., Hall, J.S., Eyres, I., Mansfield, W., and Smith, A. (2009). Klf4
874 reverts developmentally programmed restriction of ground state pluripotency.
875 Development *136*, 1063–1069.

876 13. Takahashi, S., Kobayashi, S., and Hiratani, I. (2018). Epigenetic differences between

877 naïve and primed pluripotent stem cells. Cell. Mol. Life Sci. *75*, 1191–1203.

878 14. Bao, S., Tang, F., Li, X., Hayashi, K., Gillich, A., Lao, K., and Surani, M.A. (2009).
879 Epigenetic reversion of post-implantation epiblast to pluripotent embryonic stem cells.
880 Nature *461*, 1292–1295.

881 15. Habibi, E., Brinkman, A.B., Arand, J., Kroeze, L.I., Kerstens, H.H.D., Matarese, F.,
882 Lepikhov, K., Gut, M., Brun-Heath, I., Hubner, N.C., et al. (2013). Whole-genome
883 bisulfite sequencing of two distinct interconvertible DNA methylomes of mouse
884 embryonic stem cells. Cell Stem Cell *13*, 360–369.

885 16. Leitch, H.G., McEwen, K.R., Turp, A., Encheva, V., Carroll, T., Grabole, N., Mansfield, W.,
886 Nashun, B., Knezovich, J.G., Smith, A., et al. (2013). Naive pluripotency is associated
887 with global DNA hypomethylation. Nat. Struct. Mol. Biol. *20*, 311–316.

888 17. Singer, Z.S., Yong, J., Tischler, J., Hackett, J.A., Altinok, A., Surani, M.A., Cai, L., and
889 Elowitz, M.B. (2014). Dynamic heterogeneity and DNA methylation in embryonic stem
890 cells. Mol. Cell *55*, 319–331.

891 18. Factor, D.C., Corradin, O., Zentner, G.E., Saiakhova, A., Song, L., Chenoweth, J.G.,
892 McKay, R.D., Crawford, G.E., Scacheri, P.C., and Tesar, P.J. (2014). Epigenomic
893 comparison reveals activation of "seed" enhancers during transition from naive to
894 primed pluripotency. Cell Stem Cell *14*, 854–863.

895 19. Buecker, C., Srinivasan, R., Wu, Z., Calo, E., Acampora, D., Faial, T., Simeone, A., Tan,
896 M., Swigut, T., and Wysocka, J. (2014). Reorganization of enhancer patterns in
897 transition from naive to primed pluripotency. Cell Stem Cell *14*, 838–853.

898 20. Gerondakis, S., Grumont, R., Gugasyan, R., Wong, L., Isomura, I., Ho, W., and Banerjee,
899 A. (2006). Unravelling the complexities of the NF-kappaB signalling pathway using
900 mouse knockout and transgenic models. Oncogene *25*, 6781–6799.

901 21. Kaltschmidt, C., Greiner, J.F.W., and Kaltschmidt, B. (2021). The Transcription Factor
902 NF-κB in Stem Cells and Development. Cells *10*. 10.3390/cells10082042.

903 22. Espín-Palazón, R., and Traver, D. (2016). The NF-κB family: Key players during
904 embryonic development and HSC emergence. Exp. Hematol. *44*, 519–527.

905 23. Li, S., Sun, J., Zhang, B.-W., Yang, L., Wan, Y.-C., Chen, B.-B., Xu, N., Xu, Q.-R., Fan, J.,
906 Shang, J.-N., et al. (2024). ATG5 attenuates inflammatory signaling in mouse embryonic
907 stem cells to control differentiation. Dev. Cell. 10.1016/j.devcel.2024.01.026.

908 24. Torres, J., and Watt, F.M. (2008). Nanog maintains pluripotency of mouse embryonic
909 stem cells by inhibiting NFkappaB and cooperating with Stat3. Nat. Cell Biol. *10*, 194–
910 201.

911 25. Dutta, D., Ray, S., Home, P., Larson, M., Wolfe, M.W., and Paul, S. (2011). Self-renewal
912 versus lineage commitment of embryonic stem cells: protein kinase C signaling shifts
913 the balance. Stem Cells *29*, 618–628.

26. Zhang, Q., Lenardo, M.J., and Baltimore, D. (2017). 30 Years of NF-κB: A Blossoming of Relevance to Human Pathobiology. Cell *168*, 37–57.

27. Mulero, M.C., Ferres-Marco, D., Islam, A., Margalef, P., Pecoraro, M., Toll, A., Drechsel, N., Charneco, C., Davis, S., Bellora, N., et al. (2013). Chromatin-bound IκBα regulates a subset of polycomb target genes in differentiation and cancer. Cancer Cell *24*, 151–166.

28. Marruecos, L., Bertran, J., Guillén, Y., González, J., Batlle, R., López-Arribillaga, E., Garrido, M., Ruiz-Herguido, C., Lisiero, D., González-Farré, M., et al. (2020). IκBα deficiency imposes a fetal phenotype to intestinal stem cells. EMBO Rep. *21*, e49708.

29. Marruecos, L., Bertran, J., Álvarez-Villanueva, D., Mulero, M.C., Guillén, Y., Palma, L.G., Floor, M., Vert, A., Arce-Gallego, S., Pecharroman, I., et al. (2021). Dynamic chromatin association of IκBα is regulated by acetylation and cleavage of histone H4. EMBO Rep. *22*, e52649.

30. Thambyrajah, R., Maqueda, M., Fadlullah, M.Z., Proffitt, M., Neo, W.H., Guillén, Y., Casado-Pelaez, M., Herrero-Molinero, P., Brujas, C., Castelluccio, N., et al. (2024). IκBα controls dormancy in hematopoietic stem cells via retinoic acid during embryonic development. Nat. Commun. *15*, 4673.

31. Aguilera, C., Hoya-Arias, R., Haegeman, G., Espinosa, L., and Bigas, A. (2004). Recruitment of IκBα to the *hes1* promoter is associated with transcriptional repression. Proceedings of the National Academy of Sciences *101*, 16537–16542.

32. Alvarez-Villanueva, D., Galan, L., Bertran, J., and Floor, M. (2023). Separation-of-function mutants reveal the NF-κB-independent involvement of IκBα in the regulation of stem cell and oncogenic programs. bioRxiv.

33. Atlasi, Y., Jafarnejad, S.M., Gkogkas, C.G., Vermeulen, M., Sonenberg, N., and Stunnenberg, H.G. (2020). The translational landscape of ground state pluripotency. Nat. Commun. *11*, 1617.

34. Tian, T.V., Di Stefano, B., Stik, G., Vila-Casadesús, M., Sardina, J.L., Vidal, E., Dasti, A., Segura-Morales, C., De Andrés-Aguayo, L., Gómez, A., et al. (2019). Whsc1 links pluripotency exit with mesendoderm specification. Nat. Cell Biol. *21*, 824–834.

35. Ghimire, S., Van der Jeught, M., Neupane, J., Roost, M.S., Anckaert, J., Popovic, M., Van Nieuwerburgh, F., Mestdagh, P., Vandesompele, J., Deforce, D., et al. (2018). Comparative analysis of naive, primed and ground state pluripotency in mouse embryonic stem cells originating from the same genetic background. Sci. Rep. *8*, 5884.

36. Zhou, W., Hinoue, T., Barnes, B., Mitchell, O., Iqbal, W., Lee, S.M., Foy, K.K., Lee, K.-H., Moyer, E.J., VanderArk, A., et al. (2022). DNA methylation dynamics and dysregulation delineated by high-throughput profiling in the mouse. Cell Genom *2*. 10.1016/j.xgen.2022.100144.

37. Choi, J., Huebner, A.J., Clement, K., Walsh, R.M., Savol, A., Lin, K., Gu, H., Di Stefano, B., Brumbaugh, J., Kim, S.-Y., et al. (2017). Prolonged Mek1/2 suppression impairs the

952 developmental potential of embryonic stem cells. Nature *548*, 219–223.

953 38. Di Stefano, B., Luo, E.-C., Haggerty, C., Aigner, S., Charlton, J., Brumbaugh, J., Ji, F.,
954 Rabano Jiménez, I., Clowers, K.J., Huebner, A.J., et al. (2019). The RNA Helicase DDX6
955 Controls Cellular Plasticity by Modulating P-Body Homeostasis. Cell Stem Cell *25*, 622–
956 638.e13.

957 39. Brena, D., Bertran, J., Porta-de-la-Riva, M., Guillén, Y., Cornes, E., Kukhtar, D., Campos-
958 Vicens, L., Fernández, L., Pecharroman, I., García-López, A., et al. (2020). Ancestral
959 function of Inhibitors-of-kappaB regulates Caenorhabditis elegans development. Sci.
960 Rep. *10*, 16153.

961 40. Hayden, M.S., and Ghosh, S. (2008). Shared principles in NF-kappaB signaling. Cell *132*,
962 344–362.

963 41. Basak, S., Kim, H., Kearns, J.D., Tergaonkar, V., O'Dea, E., Werner, S.L., Benedict, C.A.,
964 Ware, C.F., Ghosh, G., Verma, I.M., et al. (2007). A fourth IkappaB protein within the
965 NF-kappaB signaling module. Cell *128*, 369–381.

966 42. Thambyrajah, R., Fadlullah, Z., Proffitt, M., Neo, W.H., Guillén, Y., Casado-Pelaez, M.,
967 Herrero-Molinero, P., Brujas, C., Castelluccio, N., González, J., et al. (2022). IκBα
968 controls dormancy induction in Hematopoietic stem cell development via retinoic acid.
969 bioRxiv, 2022.11.17.516971. 10.1101/2022.11.17.516971.

970 43. Álvarez-Villanueva, D., Galán-Palma, L., Bertran, J., Floor, M., Solé, L., Lobo-Jarne, T.,
971 Maqueda, M., Rajbhandari, R., Marruecos, L., Villà-Freixa, J., et al. (2023). Separation-
972 of-function mutants reveal the NF-κB-independent involvement of IκBα in the
973 regulation of stem cell and oncogenic programs. bioRxiv, 2023.06.21.545928.
974 10.1101/2023.06.21.545928.

975 44. Guo, Y.-L. (2019). The underdeveloped innate immunity in embryonic stem cells: The
976 molecular basis and biological perspectives from early embryogenesis. Am. J. Reprod.
977 Immunol. *81*, e13089.

978 45. Pantier, R., Tatar, T., Colby, D., and Chambers, I. (2019). Endogenous epitope-tagging of
979 Tet1, Tet2 and Tet3 identifies TET2 as a naïve pluripotency marker. Life Sci Alliance *2*.
980 10.26508/lsa.201900516.

981 46. Sroczynska, P., Lancrin, C., Pearson, S., Kouskoff, V., and Lacaud, G. (2009). In vitro
982 differentiation of mouse embryonic stem cells as a model of early hematopoietic
983 development. Methods Mol. Biol. *538*, 317–334.

984 47. Chen, Q., Luo, W., Veach, R.A., Hickman, A.B., Wilson, M.H., and Dyda, F. (2020).
985 Structural basis of seamless excision and specific targeting by piggyBac transposase.
986 Nat. Commun. *11*, 3446.

987 48. Schneider, C.A., Rasband, W.S., and Eliceiri, K.W. (2012). NIH Image to ImageJ: 25 years
988 of image analysis. Nat. Methods *9*, 671–675.

989 49. Ewels, P., Afyounian, E., and Schuster-Boeckler, B.F.K. (2012). TrimGalore: v0. 6.7-DOI
990 via Zenodo.(Zenodo, 2021). doi: 10.5281/zenodo. 5127899. 2. Langmead, B. & Salzberg,
991 SL Fast gapped-read alignment with …. Nat. Methods.

992 50. Langmead, B., and Salzberg, S.L. (2012). Fast gapped-read alignment with Bowtie 2.
993 Nat. Methods *9*, 357–359.

994 51. Danecek, P., Bonfield, J.K., Liddle, J., Marshall, J., Ohan, V., Pollard, M.O., Whitwham,
995 A., Keane, T., McCarthy, S.A., Davies, R.M., et al. (2021). Twelve years of SAMtools and
996 BCFtools. Gigascience *10*. 10.1093/gigascience/giab008.

997 52. Landt, S.G., Marinov, G.K., Kundaje, A., Kheradpour, P., Pauli, F., Batzoglou, S.,
998 Bernstein, B.E., Bickel, P., Brown, J.B., Cayting, P., et al. (2012). ChIP-seq guidelines and
999 practices of the ENCODE and modENCODE consortia. Genome Res. *22*, 1813–1831.

1000 53. Ramírez, F., Ryan, D.P., Grüning, B., Bhardwaj, V., Kilpert, F., Richter, A.S., Heyne, S.,
1001 Dündar, F., and Manke, T. (2016). deepTools2: a next generation web server for deep-
1002 sequencing data analysis. Nucleic Acids Res. *44*, W160–W165.

1003 54. Stovner, E.B., and Sætrom, P. (2019). epic2 efficiently finds diffuse domains in ChIP-seq
1004 data. Bioinformatics *35*, 4392–4393.

1005 55. Zhang, Y., Liu, T., Meyer, C.A., Eeckhoute, J., Johnson, D.S., Bernstein, B.E., Nusbaum,
1006 C., Myers, R.M., Brown, M., Li, W., et al. (2008). Model-based analysis of ChIP-Seq
1007 (MACS). Genome Biol. *9*, R137.

1008 56. Stark, R., Brown, G., and Others (2011). DiffBind: differential binding analysis of ChIP-
1009 Seq peak data. R package version *100*.

1010 57. Gu, Z., Eils, R., Schlesner, M., and Ishaque, N. (2018). EnrichedHeatmap: an
1011 R/Bioconductor package for comprehensive visualization of genomic signal
1012 associations. BMC Genomics *19*, 234.

1013 58. Robinson, J.T., Thorvaldsdóttir, H., Winckler, W., Guttman, M., Lander, E.S., Getz, G.,
1014 and Mesirov, J.P. (2011). Integrative genomics viewer. Nat. Biotechnol. *29*, 24–26.

1015 59. Liao, Y., Smyth, G.K., and Shi, W. (2014). featureCounts: an efficient general purpose
1016 program for assigning sequence reads to genomic features. Bioinformatics *30*, 923–
1017 930.

1018 60. Love, M.I., Huber, W., and Anders, S. (2014). Moderated estimation of fold change and
1019 dispersion for RNA-seq data with DESeq2. Genome Biol. *15*, 550.

1020 61. Zhu, A., Ibrahim, J.G., and Love, M.I. (2019). Heavy-tailed prior distributions for
1021 sequence count data: removing the noise and preserving large differences.
1022 Bioinformatics *35*, 2084–2092.

1023 62. Benjamini, Y., and Hochberg, Y. (1995). Controlling the False Discovery Rate: A Practical
1024 and Powerful Approach to Multiple Testing. J. R. Stat. Soc. Series B Stat. Methodol. *57*,

1025 289–300.

1026 63. Garcia-Prieto, C.A., Álvarez-Errico, D., Musulen, E., Bueno-Costa, A., N. Vazquez, B.,
1027 Vaquero, A., and Esteller, M. (2022). Validation of a DNA methylation microarray for
1028 285,000 CpG sites in the mouse genome. Epigenetics *17*, 1677–1685.

1029 64. Ashburner, M., Ball, C.A., Blake, J.A., Botstein, D., Butler, H., Cherry, J.M., Davis, A.P.,
1030 Dolinski, K., Dwight, S.S., Eppig, J.T., et al. (2000). Gene ontology: tool for the
1031 unification of biology. The Gene Ontology Consortium. Nat. Genet. *25*, 25–29.

1032 65. Kanehisa, M., and Goto, S. (2000). KEGG: kyoto encyclopedia of genes and genomes.
1033 Nucleic Acids Res. *28*, 27–30.

1034 66. Martens, M., Ammar, A., Riutta, A., Waagmeester, A., Slenter, D.N., Hanspers, K., A
1035 Miller, R., Digles, D., Lopes, E.N., Ehrhart, F., et al. (2021). WikiPathways: connecting
1036 communities. Nucleic Acids Res. *49*, D613–D621.

1037 67. Hu, S., Metcalf, E., Mahat, D.B., Chan, L., Sohal, N., Chakraborty, M., Hamilton, M.,
1038 Singh, A., Singh, A., Lees, J.A., et al. (2022). Transcription factor antagonism regulates
1039 heterogeneity in embryonic stem cell states. Mol. Cell *82*, 4410–4427.e12.

1040 68. Korotkevich, G., Sukhov, V., Budin, N., Shpak, B., Artyomov, M.N., and Sergushichev, A.
1041 (2021). Fast gene set enrichment analysis. bioRxiv, 060012. 10.1101/060012.

1042 69. Zhou, W., Triche, T.J., Jr, Laird, P.W., and Shen, H. (2018). SeSAMe: reducing artifactual
1043 detection of DNA methylation by Infinium BeadChips in genomic deletions. Nucleic
1044 Acids Res. *46*, e123.

1045 70. Hänzelmann, S., Castelo, R., and Guinney, J. (2013). GSVA: gene set variation analysis
1046 for microarray and RNA-seq data. BMC Bioinformatics *14*, 7.

Figure 1

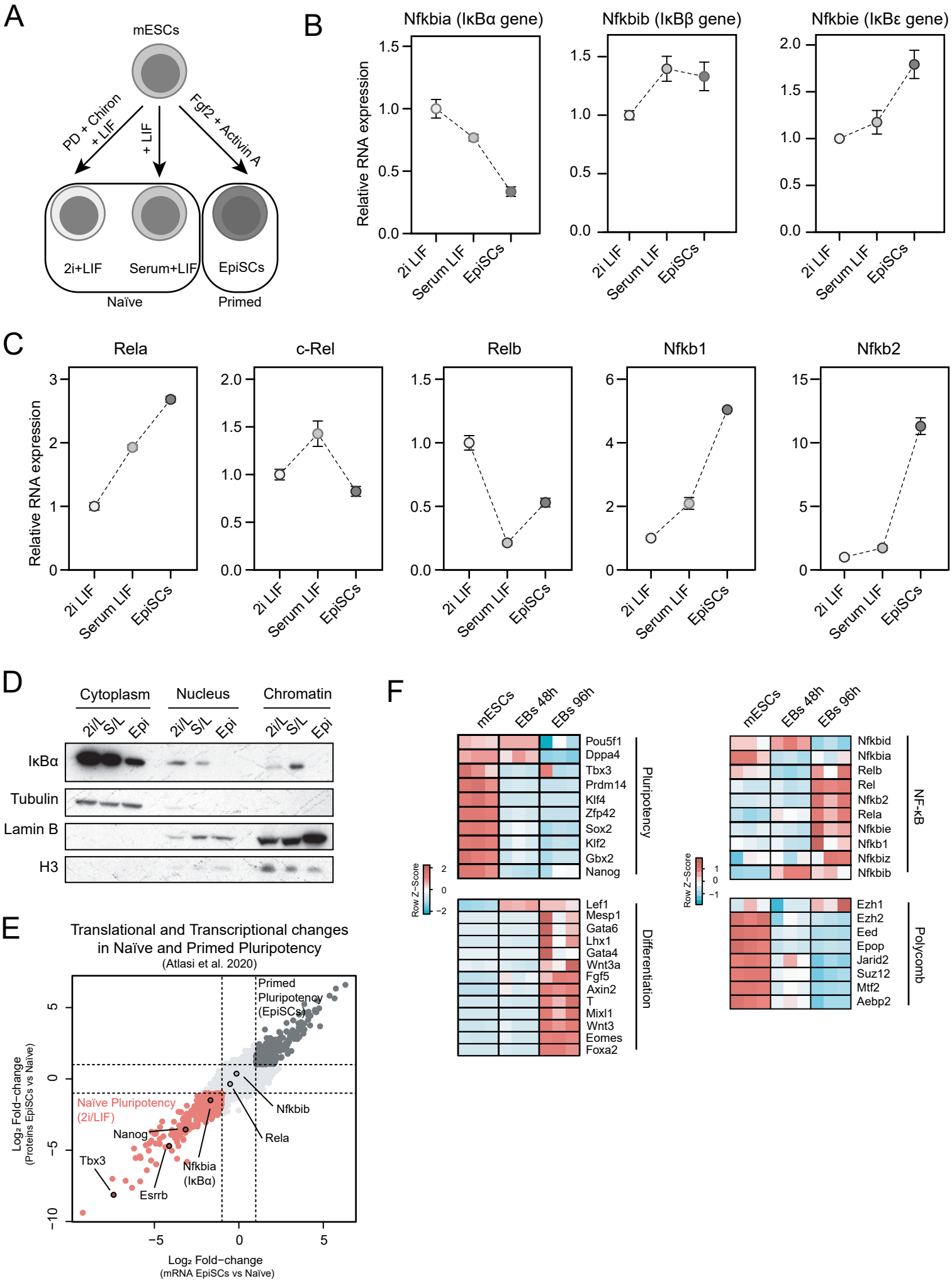
A
mESCs
PD + Chiron + LIF
+ LIF
Fgf2 + Activin A
2i+LIF
Serum+LIF
EpiSCs
Naïve
Primed
B
Nfkbia (IκBα gene)
Nfkbib (IκBβ gene)
Nfkbie (IκBε gene)
Relative RNA expression
2i LIF
Serum LIF
EpiSCs
C
Rela
c-Rel
Relb
Nfkb1
Nfkb2
Relative RNA expression
D
Cytoplasm
Nucleus
Chromatin
2i/L
S/L
Epi
IκBα
Tubulin
Lamin B
H3
E
Translational and Transcriptional changes in Naïve and Primed Pluripotency
(Atlasi et al. 2020)
Primed Pluripotency (EpiSCs)
Naïve Pluripotency (2i/LIF)
Nfkbib
Rela
Nanog
Tbx3
Nfkbia (IκBα)
Esrrb
Log₂ Fold-change (Proteins EpiSCs vs Naïve)
Log₂ Fold-change (mRNA EpiSCs vs Naïve)
F
mESCs
EBs 48h
EBs 96h
Pou5f1
Dppa4
Tbx3
Prdm14
Klf4
Zfp42
Sox2
Klf2
Gbx2
Nanog
Pluripotency
Lef1
Mesp1
Gata6
Lhx1
Gata4
Wnt3a
Fgf5
Axin2
T
Mixl1
Wnt3
Eomes
Foxa2
Differentiation
Row Z-Score
Nfkbid
Nfkbia
Relb
Rel
Nfkb2
Rela
Nfkbie
Nfkb1
Nfkbiz
Nfkbib
NF-κB
Ezh1
Ezh2
Eed
Epop
Jarid2
Suz12
Mtf2
Aebp2
Polycomb

Figure 2

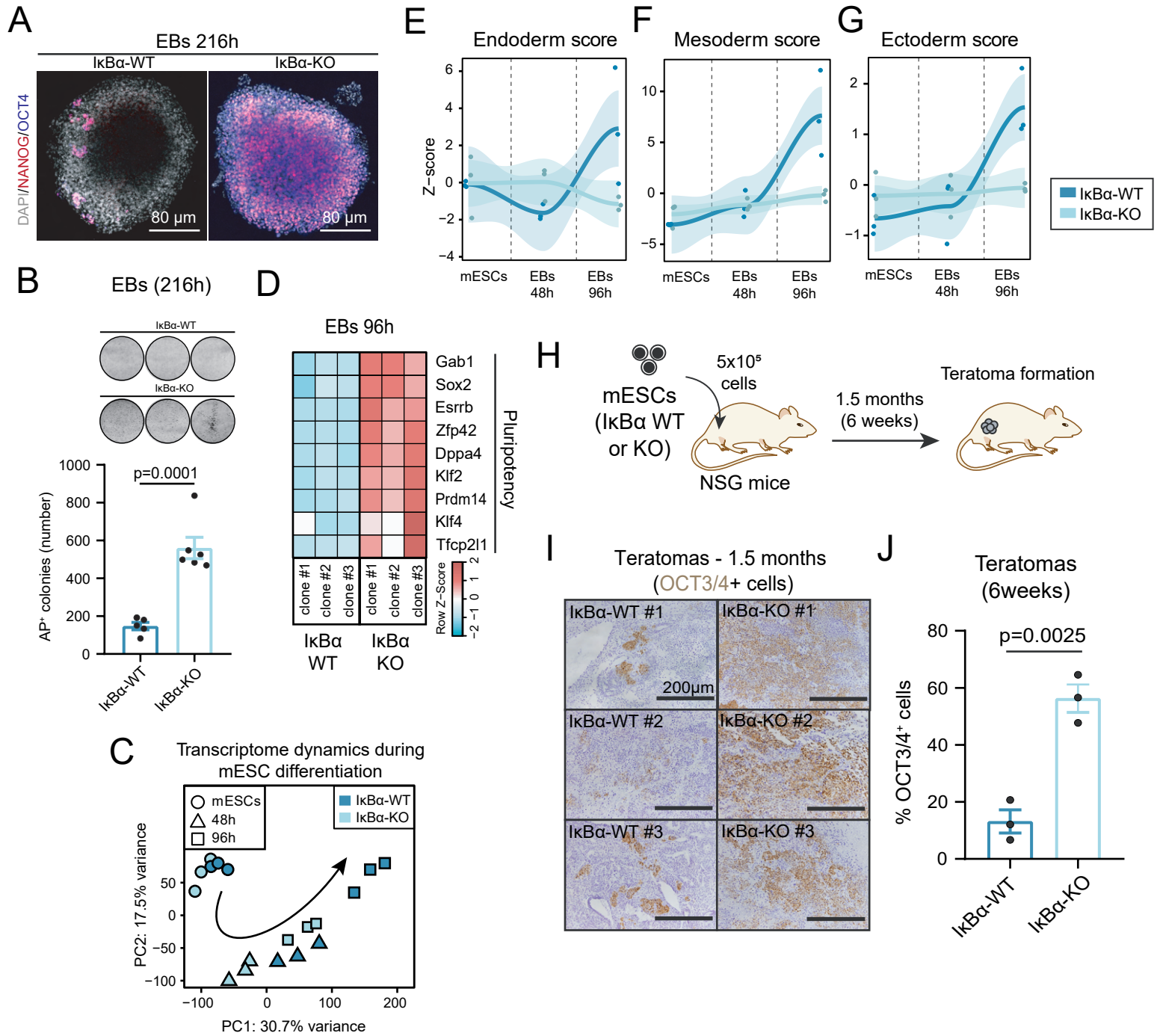
A
EBs 216h
IκBα-WT
IκBα-KO
DAPI/NANOG/OCT4
80 µm
80 µm
E
Endoderm score
Z-score
mESCs
EBs 48h
EBs 96h
F
Mesoderm score
G
Ectoderm score
IκBα-WT
IκBα-KO
B
EBs (216h)
IκBα-WT
IκBα-KO
p=0.0001
AP⁺ colonies (number)
D
EBs 96h
Gab1
Sox2
Esrrb
Zfp42
Dppa4
Klf2
Prdm14
Klf4
Tfcp2l1
Pluripotency
clone #1
clone #2
clone #3
IκBα WT
IκBα KO
Row Z-Score
H
mESCs (IκBα WT or KO)
5x10⁵ cells
NSG mice
1.5 months (6 weeks)
Teratoma formation
I
Teratomas - 1.5 months (OCT3/4+ cells)
IκBα-WT #1
IκBα-KO #1
200µm
IκBα-WT #2
IκBα-KO #2
IκBα-WT #3
IκBα-KO #3
J
Teratomas (6weeks)
p=0.0025
% OCT3/4⁺ cells
C
Transcriptome dynamics during mESC differentiation
mESCs
48h
96h
IκBα-WT
IκBα-KO
PC2: 17.5% variance
PC1: 30.7% variance

Figure 3

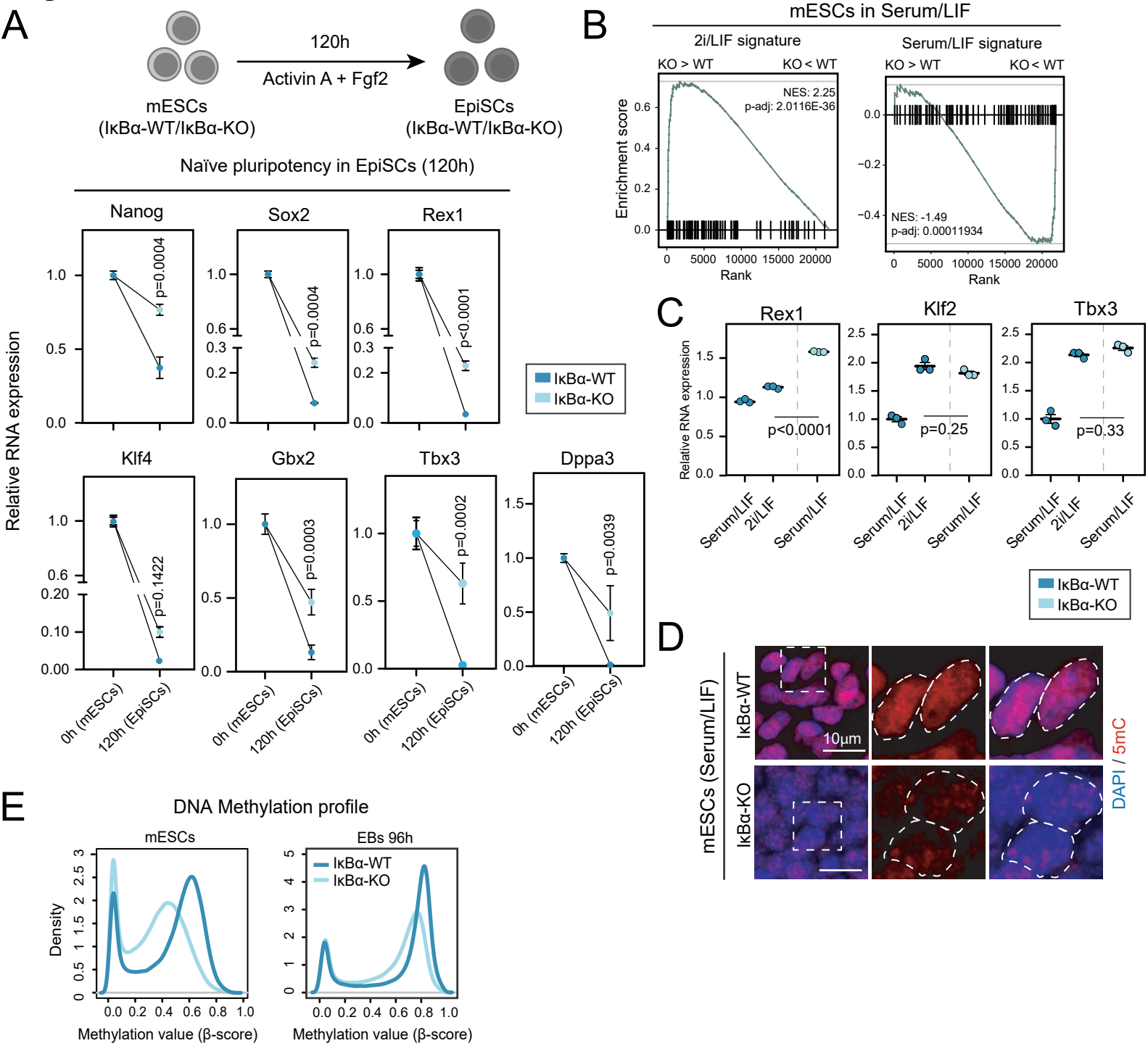
A
120h
Activin A + Fgf2
mESCs
(IκBα-WT/IκBα-KO)
EpiSCs
(IκBα-WT/IκBα-KO)
Naïve pluripotency in EpiSCs (120h)
Nanog
Sox2
Rex1
Klf4
Gbx2
Tbx3
Dppa3
Relative RNA expression
p=0.0004
p=0.0004
p<0.0001
p=0.1422
p=0.0003
p=0.0002
p=0.0039
IκBα-WT
IκBα-KO
0h (mESCs)
120h (EpiSCs)
B
mESCs in Serum/LIF
2i/LIF signature
Serum/LIF signature
KO > WT
KO < WT
NES: 2.25
p-adj: 2.0116E-36
NES: -1.49
p-adj: 0.00011934
Enrichment score
Rank
C
Rex1
Klf2
Tbx3
Relative RNA expression
p<0.0001
p=0.25
p=0.33
Serum/LIF
2i/LIF
Serum/LIF
IκBα-WT
IκBα-KO
D
mESCs (Serum/LIF)
IκBα-WT
IκBα-KO
10μm
DAPI / 5mC

E
DNA Methylation profile
mESCs
EBs 96h
IκBα-WT
IκBα-KO
Density
Methylation value (β-score)

Figure 4

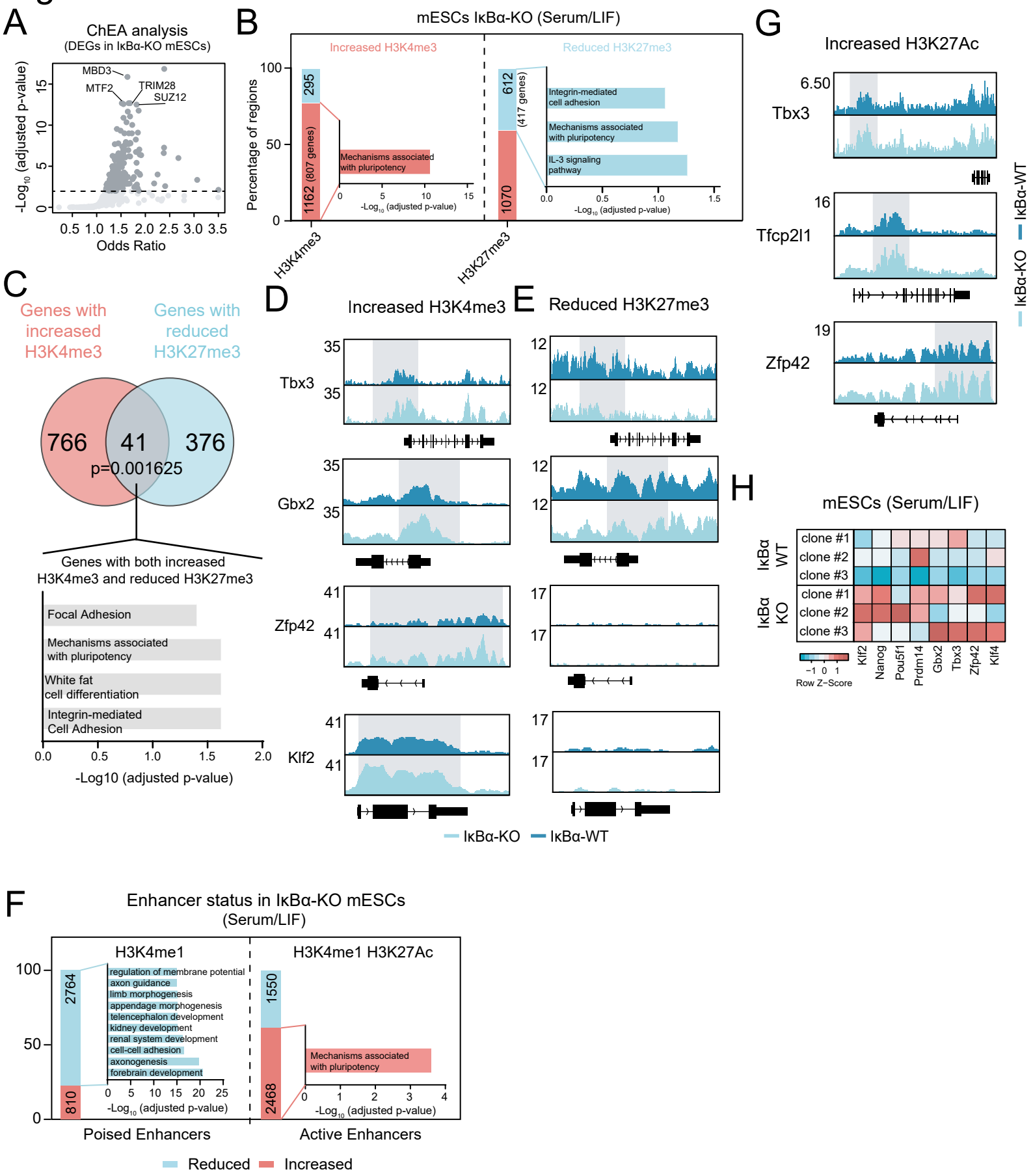
A
ChEA analysis
(DEGs in IκBα-KO mESCs)
MBD3
MTF2
TRIM28
SUZ12
-Log10 (adjusted p-value)
Odds Ratio
B
mESCs IκBα-KO (Serum/LIF)
Increased H3K4me3
Reduced H3K27me3
Percentage of regions
295
1162 (807 genes)
612
(417 genes)
1070
Mechanisms associated with pluripotency
Integrin-mediated cell adhesion
Mechanisms associated with pluripotency
IL-3 signaling pathway
-Log10 (adjusted p-value)
H3K4me3
H3K27me3
C
Genes with increased H3K4me3
Genes with reduced H3K27me3
766
41
376
p=0.001625
Genes with both increased H3K4me3 and reduced H3K27me3
Focal Adhesion
Mechanisms associated with pluripotency
White fat cell differentiation
Integrin-mediated Cell Adhesion
-Log10 (adjusted p-value)
D
Increased H3K4me3
E
Reduced H3K27me3
Tbx3
Gbx2
Zfp42
Klf2
IκBα-KO
IκBα-WT
G
Increased H3K27Ac
Tbx3
Tfcp2l1
Zfp42
IκBα-KO
IκBα-WT
H
mESCs (Serum/LIF)
IκBα WT
IκBα KO
clone #1
clone #2
clone #3
Klf2
Nanog
Pou5f1
Prdm14
Gbx2
Tbx3
Zfp42
Klf4
Row Z-Score
F
Enhancer status in IκBα-KO mESCs
(Serum/LIF)
H3K4me1
H3K4me1 H3K27Ac
2764
810
1550
2468
regulation of membrane potential
axon guidance
limb morphogenesis
appendage morphogenesis
telencephalon development
kidney development
renal system development
cell-cell adhesion
axonogenesis
forebrain development
Mechanisms associated with pluripotency
-Log10 (adjusted p-value)
Poised Enhancers
Active Enhancers
Reduced
Increased

Figure 5

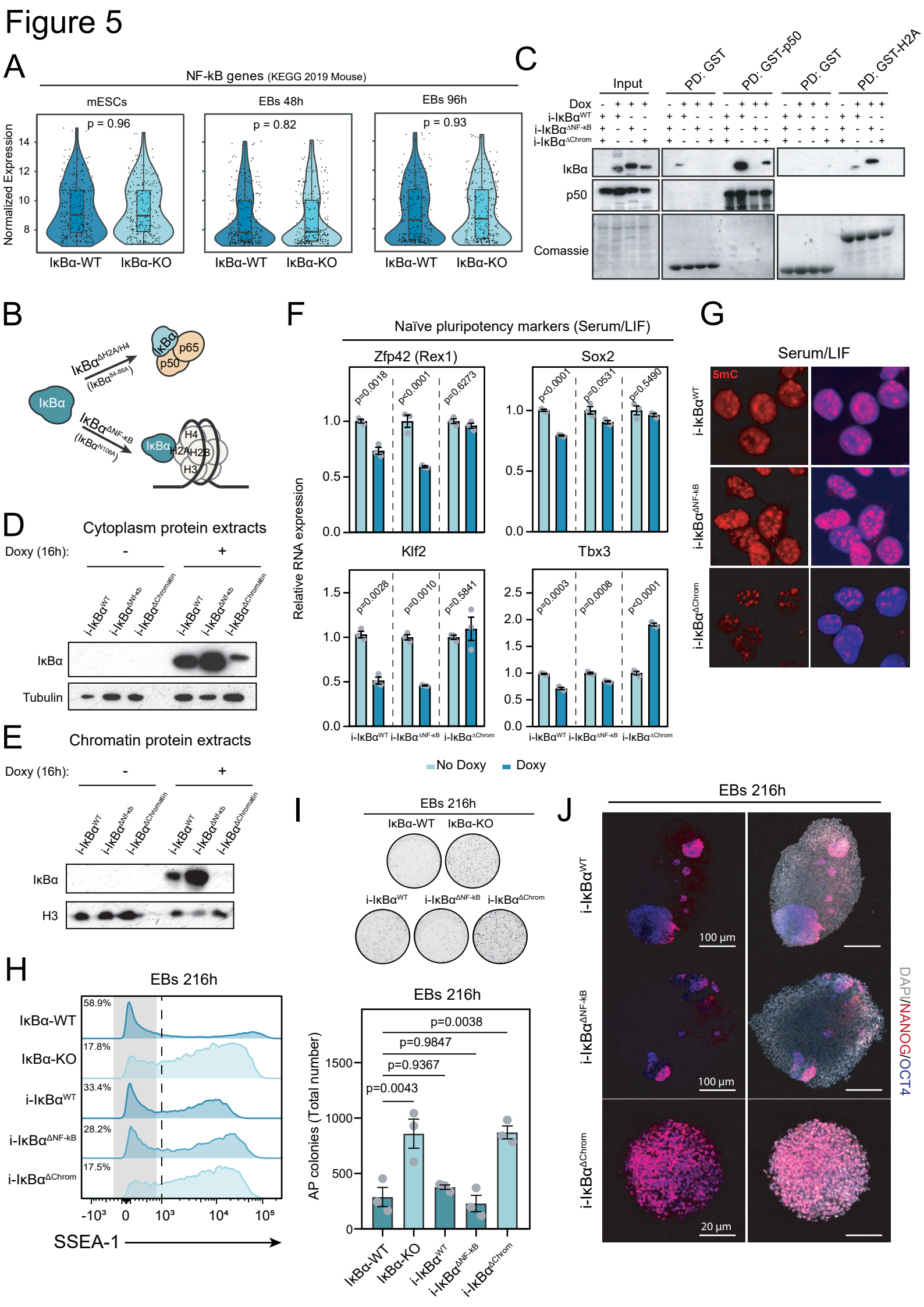
A
NF-kB genes (KEGG 2019 Mouse)
mESCs
EBs 48h
EBs 96h
p = 0.96
p = 0.82
p = 0.93
Normalized Expression
IκBα-WT
IκBα-KO
B
IκBα
IκBα^ΔH2A/H4
(IκBα^84-86A)
p65
p50
IκBα^ΔNF-κB
(IκBα^N108A)
H4
H2A
H2B
H3
C
Input
PD: GST
PD: GST-p50
PD: GST
PD: GST-H2A
Dox
i-IκBα^WT
i-IκBα^ΔNF-κB
i-IκBα^ΔChrom
IκBα
p50
Comassie
D
Cytoplasm protein extracts
Doxy (16h):
-
+
i-IκBα^WT
i-IκBα^ΔNF-κB
i-IκBα^ΔChromatin
IκBα
Tubulin
E
Chromatin protein extracts
Doxy (16h):
-
+
i-IκBα^WT
i-IκBα^ΔNF-κB
i-IκBα^ΔChromatin
IκBα
H3
F
Naïve pluripotency markers (Serum/LIF)
Zfp42 (Rex1)
Sox2
Klf2
Tbx3
Relative RNA expression
p=0.0018
p<0.0001
p=0.6273
p<0.0001
p=0.0531
p=0.5490
p=0.0028
p=0.0010
p=0.5841
p=0.0003
p=0.0008
p<0.0001
i-IκBα^WT
i-IκBα^ΔNF-κB
i-IκBα^ΔChrom
No Doxy
Doxy
G
Serum/LIF
5mC
i-IκBα^WT
i-IκBα^ΔNF-κB
i-IκBα^ΔChrom
H
EBs 216h
IκBα-WT
IκBα-KO
i-IκBα^WT
i-IκBα^ΔNF-κB
i-IκBα^ΔChrom
58.9%
17.8%
33.4%
28.2%
17.5%
SSEA-1
I
EBs 216h
IκBα-WT
IκBα-KO
i-IκBα^WT
i-IκBα^ΔNF-κB
i-IκBα^ΔChrom
EBs 216h
AP colonies (Total number)
p=0.0038
p=0.9847
p=0.9367
p=0.0043
J
EBs 216h
i-IκBα^WT
i-IκBα^ΔNF-κB
i-IκBα^ΔChrom
100 µm
100 µm
20 µm
DAPI/NANOG/OCT4

Figure S1 Related to Figure 2

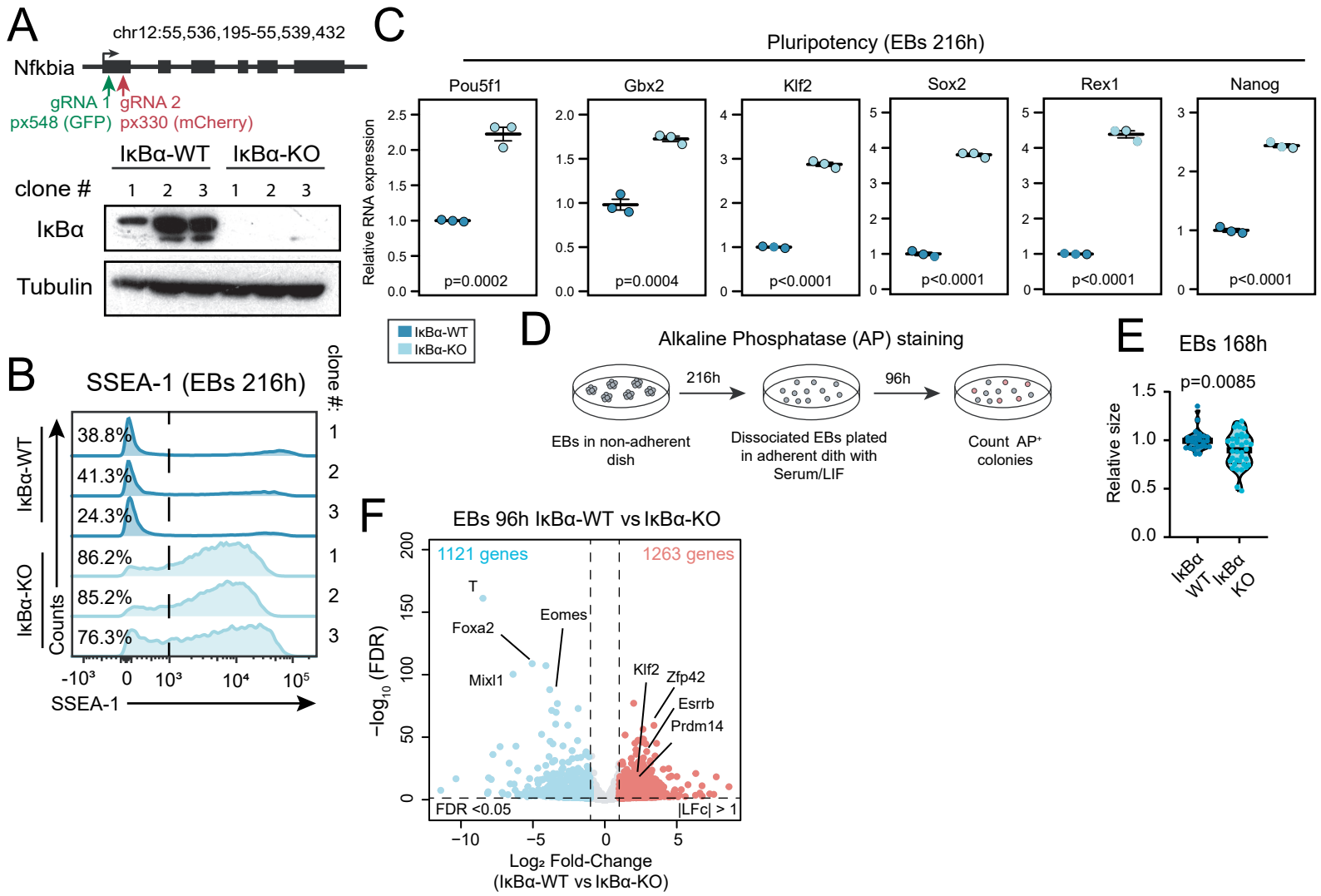

Figure S2 related to figure 3

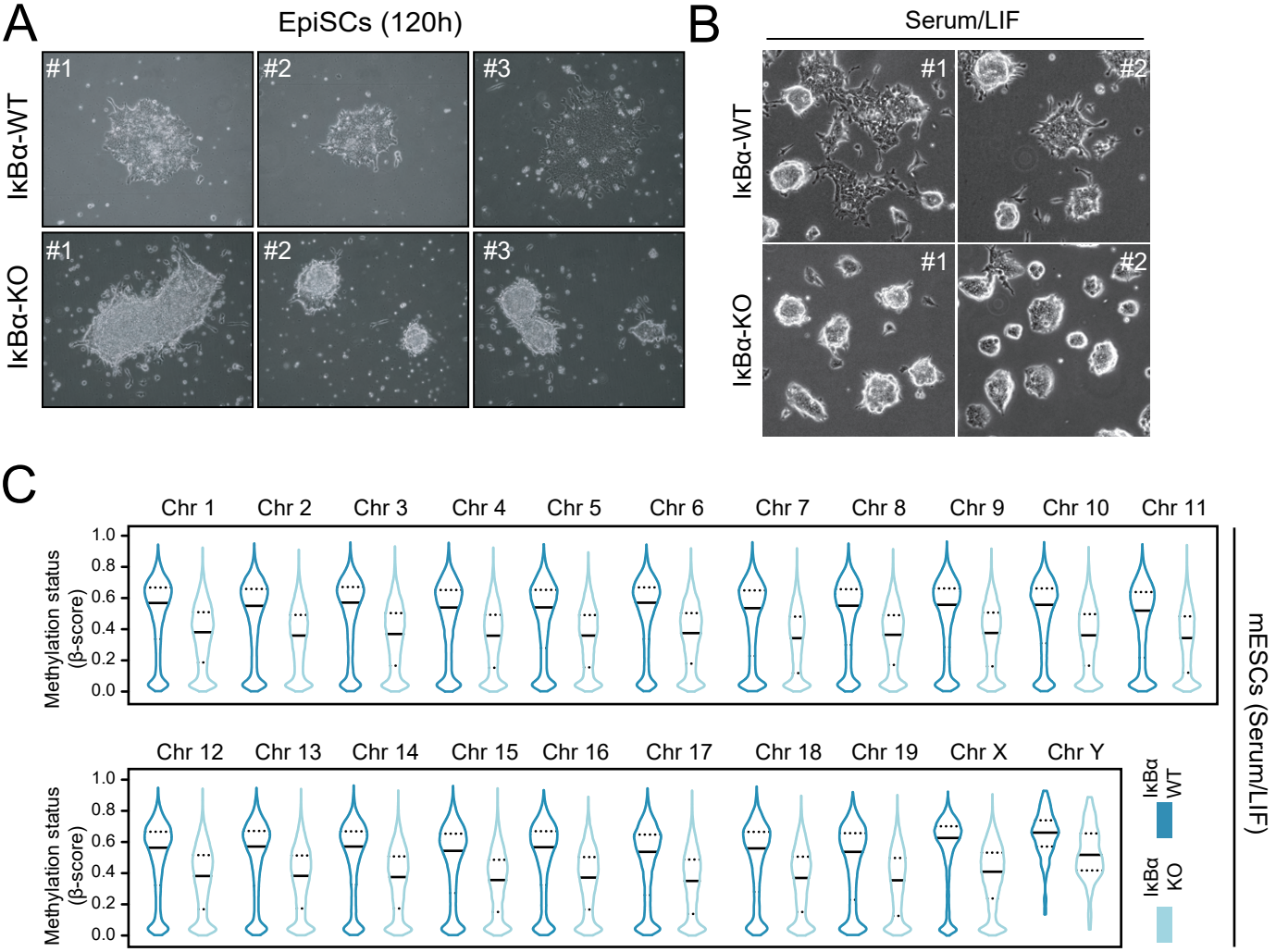

Figure S3 related to figure 4

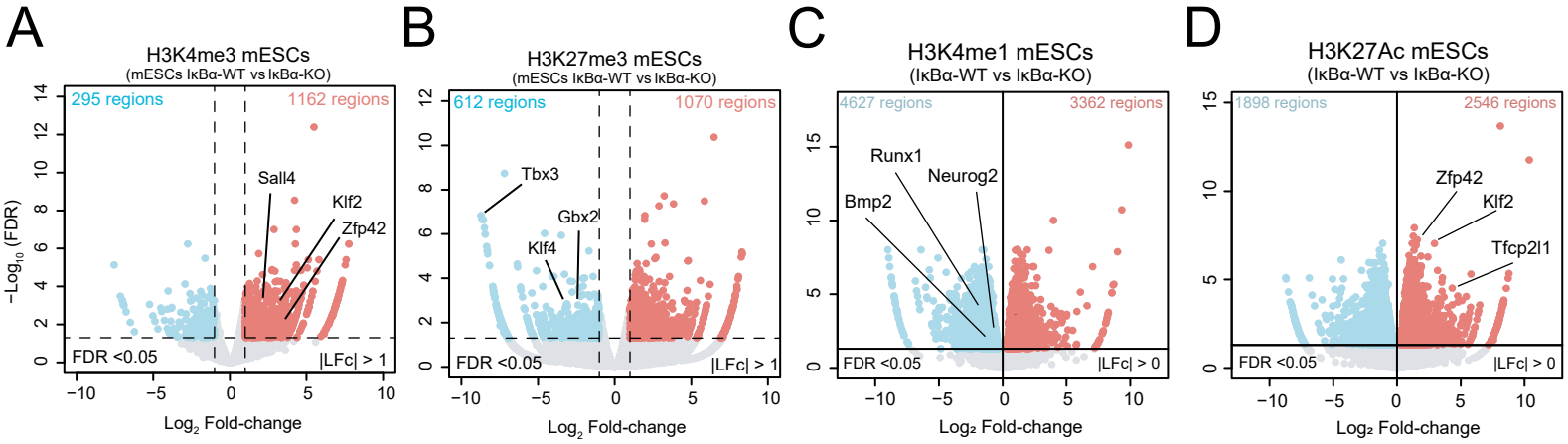
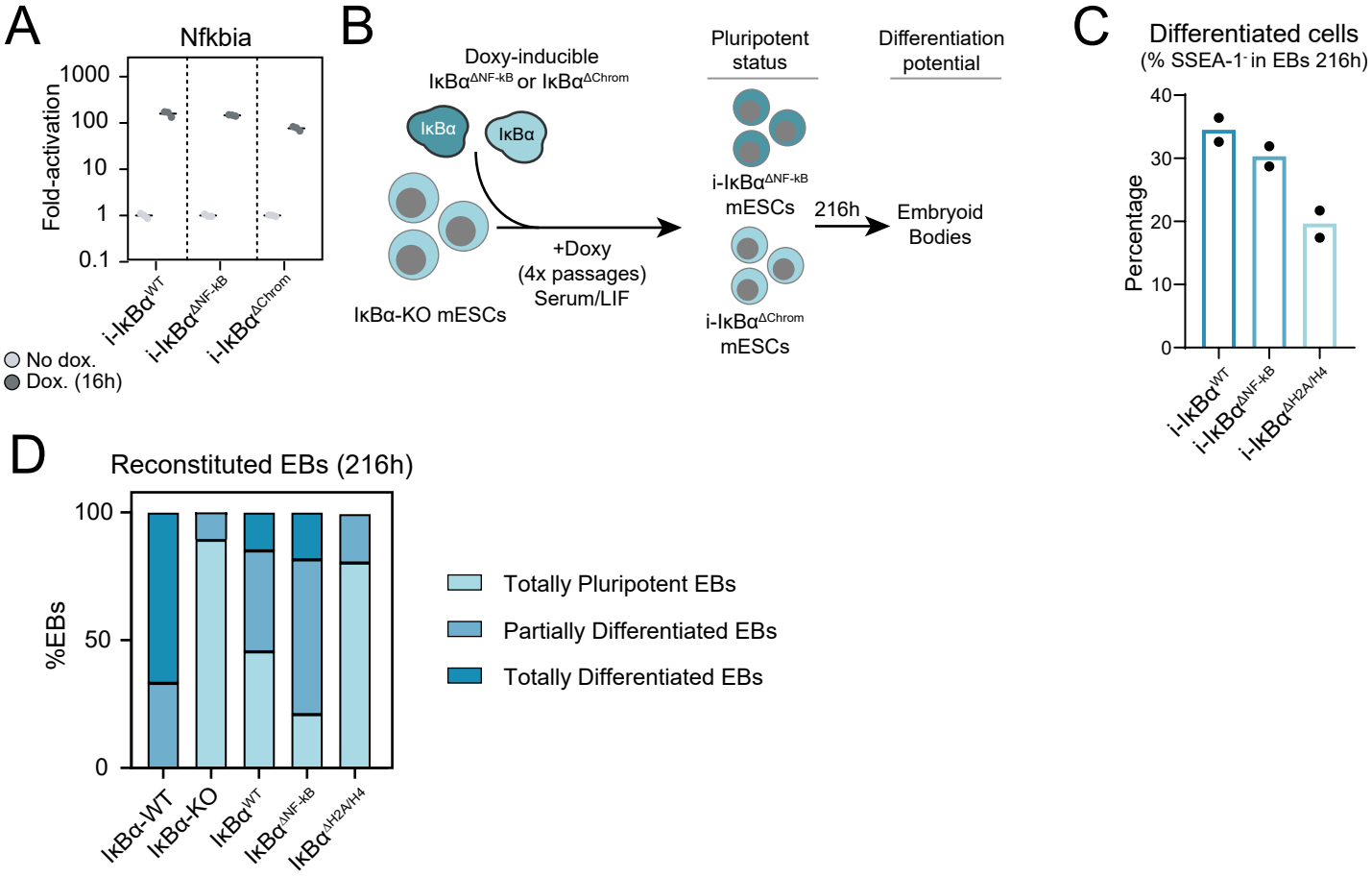
Figure S4 related to figure 5